Using SMOS and Sentinel 3 satellite data to obtain high resolution soil moisture maps.

Cristina González Delgado

May 21, 2019

ABSTRACT

Surface soil moisture is a critical climate variable and strongly influences water and energy cycles at the surface-atmosphere interface. It is widely used to improve numerical climate and weather models, rainfall and drough estimation, vegetation monitoring, among others.

Traditionally, there were two main ways to retrieve soil moisture data. On one hand, soil moisture sensors networks placed and maintained in situ to obtain long term distributed measurements, which is expensive and time-consuming. On the other hand, soil moisture data could be obtained by using numerical model products combined with ground observations. But, in both cases, the data resolution provided was not enough to characterize soil moisture at large scale.

Nowadays, microwave remote sensing allows the global monitoring of soil moisture. SMOS (Soil Moisture and Ocean Salinity) mission, launched in 2009, was the first mission with this objective and providing an acceptable spatial resolution. It aims to monitor soil moisture over land surfaces, surface salinity over the oceans, and surfaces covered by snow and ice, by performing microwave radiometric measurements at L-band, characterized by being unaffected by cloud cover and variable surface solar illumination.

The SMOS soil moisture data has a spatial resolution of 35-50 km, which is enough for global applications. But, local applications such as hydrological, fire prevention, agricultural and water management, require higher soil moisture resolution. In order to cover this necessity, several downscaling methodologies have been developed to improve the spatial resolution.

The Department of Signal Theory in the UPC developed a downscaling algorithm based on the synergistic usage of low resolution soil moisture map and data provided by other satellites, that computed soil moisture maps at 1 km resolution (Maria Piles, 2010 [32]). This algorithm combines the SMOS soil moisture with NDVI and LST measurements from Aqua and Terra missions obtained by MODIS instrument.
Later, this algorithm was improved by using an adaptive sliding window, which is the version we will use in this project (Gerard Portal, 2017 [24]).

The aim of this project is to substitute the NDVI and LST measurements from MODIS used as ancillary data in the downscaling algorithm by the ones provided by Sentinel 3, comparing its differences and the variation of the high resolution soil moisture maps (SM HR maps) obtained. Also, it will include the evaluation of the data download and preparation process workflow.

ACKNOWLEDGEMENTS

First, I would like to thank my thesis supervisor Merce Val-llossera, for his advice and his close and patient attitude to me, given the tight schedule we had. Merce has guided me throughout this project and has always been willing to help.

Also, I would like to thank my family and partner, Ferran, for their unconditional support throughout this period, completely indispensable.

LIST OF FIGURES

ACRONYMS

SMOS Soil Moisture and Ocean Salinity Satellite

MIRAS Microwave Imaging Radiometer using Aperture Synthesis

ESE Earth Science Enterprise

AIRS Athmospheric Infrared Sounder

AMSU-A Advanced Microwave Sounding Unit

HSB Humidity Sounder for Brazil

AMSR-E Advanced Microwave Scanning Radiometer for EOS

CERES Clouds and the Earths Radiant Energy System

MODIS Moderate-Resolution Imaging Spectroradiometer

SWIR Short-wave Infrared

TIR Thermal Infrared

ASTER Advanced Spaceborn Thermal Emission and Reflection Radiometer

VNIR Visible and Near Infrared

MISR Multi-angle Imaging Spectroradiometer

MOPITT Measurements of Pollution in the Troposphere

ESA European Space Agency

NRT Near Real Time

NTC Non Time Critical

TB Brightness Temperature

SM Soil Moisture

HR SM High Resolution Soil Moisture

LST Land Surface Temperature

NDVI Normalized Difference Vegetation Index

CONTENTS

1

INTRODUCTION

1.1 OBJECTIVE

This project has the aim of using the downscaling algorithm developed by Gerard Portal [23] to obtain high resolution soil moisture maps at local scale, using LST and NDVI products from Sentinel 3 as ancillary data instead of MODIS, and conclude whether Sentinel 3 products could replace MODIS ones in the downscaling algorithm. If they are very alike, Sentinel 3 could guarantee the continuity of MODIS products.

The downscaling algorithm allows to increase the soil moisture resolution from $\approx$ 40 km to 1 km by using synergies of the SMOS soil moisture data with LST and NDVI data from MODIS. The idea of the project is to replace this MODIS data by the LST and NDVI products provided by Sentinel 3, and to do an intercomparsion of both products.

Throughout the evaluation of LST and NDVI from MODIS and Sentinel 3, this project studies the characteristics of each platform, the download and processing of the data, the characteristics of the LST and NDVI products from MODIS and Sentinel 3 and the variation in the high resolution soil moisture maps computed by the algorithm using the data from one or the other.

1.2 STATE OF THE ART

Soil moisture is considered an Essential Climate Variable (ECV) since it plays a critical role in characterizing the Earth's climate. It influences strongly the agriculture production and vegetation patterns, since plants and crops evolution highly depend on the soil moisture conditions, the precipitation infiltration and erosion and sedimentation, and it helps to determine future climate catastrophe as droughts or floods. Also, it is critical in the land surface - atmosphere interaction, thus influencing the generation of clouds, precipitations and the temperature.

Given so, it is used to improve climate models, vegetation monitoring or climate disasters forecasting, among others.

Soil moisture can be accurately measured in situ, but this process is time-consuming and expensive, and it requires periodical measurements.
Remote sensing is an alternative to this in situ measurements of the soil moisture, less expensive and less time consuming (Kornelsen et al. [30]).

Measuring soil moisture at large scales is challenging since its spatial variation is strong due to factors such as topography, vegetation cover or meteorological conditions.

Passive microwave remote sensing of soil moisture retrieval is based on the principle that the dielectric properties of the soil influence the soil emission at the microwave band of the electromagnetic spectrum. An thus, a change in soil moisture, which implicates necessary a change in the dielectric constant of the soil, will translate to a measurable change in the soil emissivity at the microwave band of the spectrum.

Several emperical and theoretical studies explained in more detail the soil moisture and emissivity relationship and presented retrieval approaches of the soil moisture from satellite microwave observations (F. E. Geiger and D. Williams, 1972 [22]; J. E. Hipp, 1974 [25]; P. Hoekstra A. Delaney, 1974 [20]; Eagleman, J., and Lin, W. 1976 [21]; James R. Wang and T. Schmugge, 1880 [38]; Blanchard et al., 1982 [18]; Schmugge, T, 1984 [35]; Eni G. Njokul and Dara Entekhabi, 1994 [34]). The progress in the field is reported by new articles published periodically (Barrett, B.W., Dwyer, E., Whelan, P., 2009 [17]; B. T. Gouweleeuw et al., 2012 [40]).

There are several approaches to retrieve soil moisture using satellite L-band, called passive microwave remote sensing.
Some approaches use empirical methods based in statistical modeling, specifically the regression analysis to estimate the relationship between satellite data measurements and soil moisture. These approach is good enough for local areas but they struggle when applied in large-scale since they depend heavily on time and site.
Some other approaches are considered as semi-empirical (Soares, Joo Renn, Camilo. , 1997 [36];Yu, Fan Zhao, YingShi., 2011 [41]).They provide better results at large scales but the simplifications adopted are a source of inaccuracies.
Also, recently, deep neural networks have been used to build non-linear statistical models between soil moisture and satellite data without formulating the physical process first (Hu, Z xu, Linlin Yu, B., 2018 [26]). The neural network is trained using satellate data and the soil moisture grounthruth.

Recently, space agencies have stated to launch dedicated satellite missions for passive microwave soil moisture retrieval. SMOS (Soil Moisture and Ocean Salinity mission)

was launched in November 2009 by ESA, SMAP (Soil Moisture Active and Passive mission) was launched in January 2015 by NASA.

1.3 PROJECT STRUCTURE

The project is divided in six different chapters.
The first one is an introduction to the thesis, its objective, the state of the art, its structure, and the Gantt diagram of the project.
The second chapter presents the main radiometry concepts: Brightness, black and grey bodies, the Planck and Rayleigh-Jean laws and the L-band emission of land surface.
The third chapter introduces the missions SMOS, Aqua and Terra, and Sentinel 3. Also, it describes the instruments on board of each platform and the data products they provide, highlighting the ones that are used in this project.
The fourth chapter focuses on the downscaling algorithm to obtain high resolution soil moisture maps, explaining its workflow in detail and the characteristics of the input data products.
Chapter five presents the evaluation and comparison of LST and NDVI products provided by MODIS and Sentinel 3, as well as the differences in the high resolution soil moisture maps obtained when using each as ancillary data in the downscaling algorithm.
Chapter six presents the results, conclusions and future lines. Finally, chapter seven includes the budget of the project.

1.4 PROJECT GANTT DIAGRAM

Find below the Gantt diagram showing the time schedule of this project and the decoupled tasks and milestones.

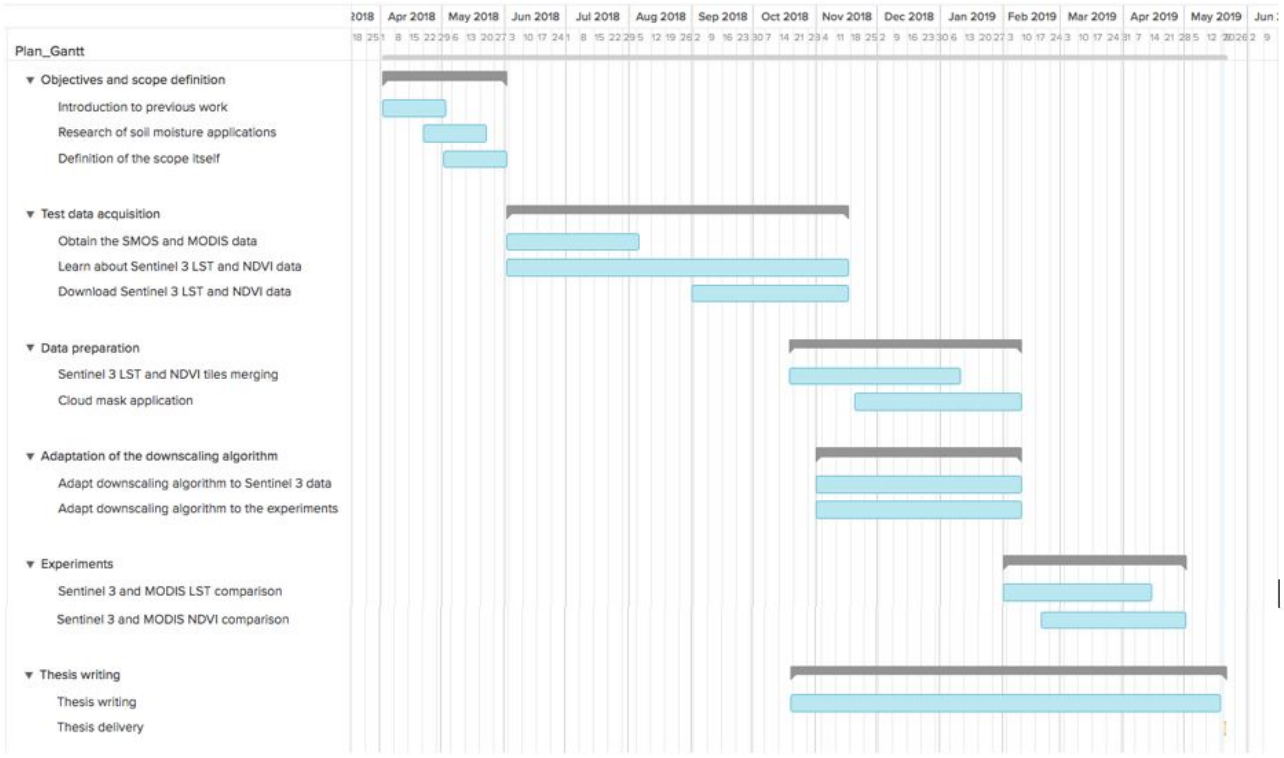

Figure 1: Project Gantt diagram

2

RADIOMETRY CONCEPTS

The Earth receives electromagnetic radiation from the sun. The atmosphere and clouds absorb part of this radiation and the remaining reaches the Earth surface, which in its turn absorbs part of this energy and the rest disperses. According to thermodynamic principles, an absorption of energy leads to an increment of the material temperature. Absorbed energy is reemited to the atmosphere when the thermal equilibrium is achieved.
The Earth's energy budget (see figure 2) represents the balance between the energy that Earth receives from the sun and the energy that it reflects back to the space.

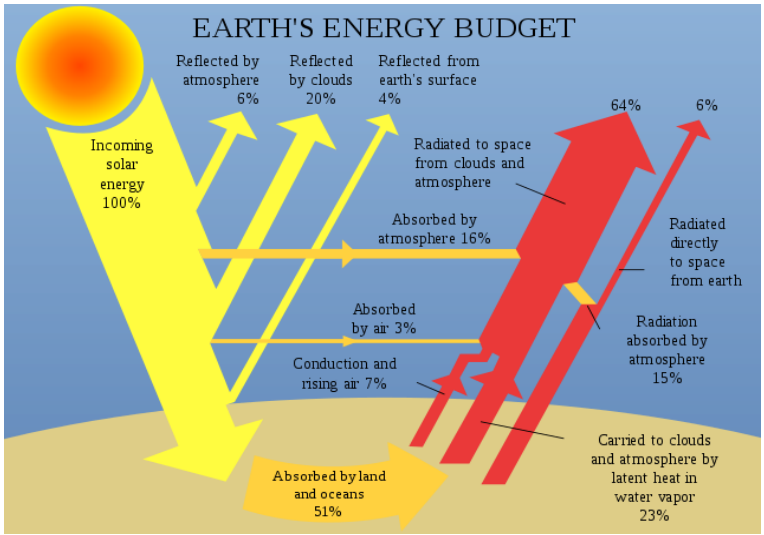

Figure 2: Earth's energy budget. Figure from [3]

This chapter reviews radiometry basic concepts, which is the science field that measures the bodies electromagnetic radiation. In addition, it presents the state of the art of soil moisture retrieval techniques.

2.1 BRIGHTNESS

Brightness or radiance B(θ, Φ)[$W.sr^{-1}.m^{-2}$] is the energy emitted from a given source, traveling in a specific direction per unit solid angle and unit projected area.

$$B(\theta, \Phi) = \frac{F_t(\theta, \Phi)}{A_t} \tag{1}$$

where $F_n(\theta, \Phi)$ is the source's normalized radiation pattern and A_t is the total radiating area.

The received power of an antenna with a finite aperture A_f and normalized radiation diagram $F_n(\theta, \Phi)$ receiving a brightness of an extended source, is calculated as shown in equation 2.

$$P = \frac{Ar}{2} \int_f^{f+\triangle f} \int \int_{4\pi} B_f(\theta, \phi) F_n(\theta, \phi) d\Omega df \tag{2}$$

where $B_f(\theta, \phi)$ is the spectral brightness per bandwidth unit df, A_r is the receiver antenna effective area, $F_n(\theta, \phi)$ is the normalized radiation pattern, Δf is the receiver antenna bandwidth, $d\Omega$ is solid radiant surface differential. The $1/2$ factor appears because the receiver antenna is polarized but not the $B_f(\theta, \phi)$, which causes that only half of the power is detected.

If we consider always the maximum of the antenna's radiation diagram and that the brightness is frequency independent, the power received by an antenna with finite aperture A_f is:

$$P = F_n \frac{A_f}{R^2} = BA \frac{A_f}{R^2} = BA_r\Omega \tag{3}$$

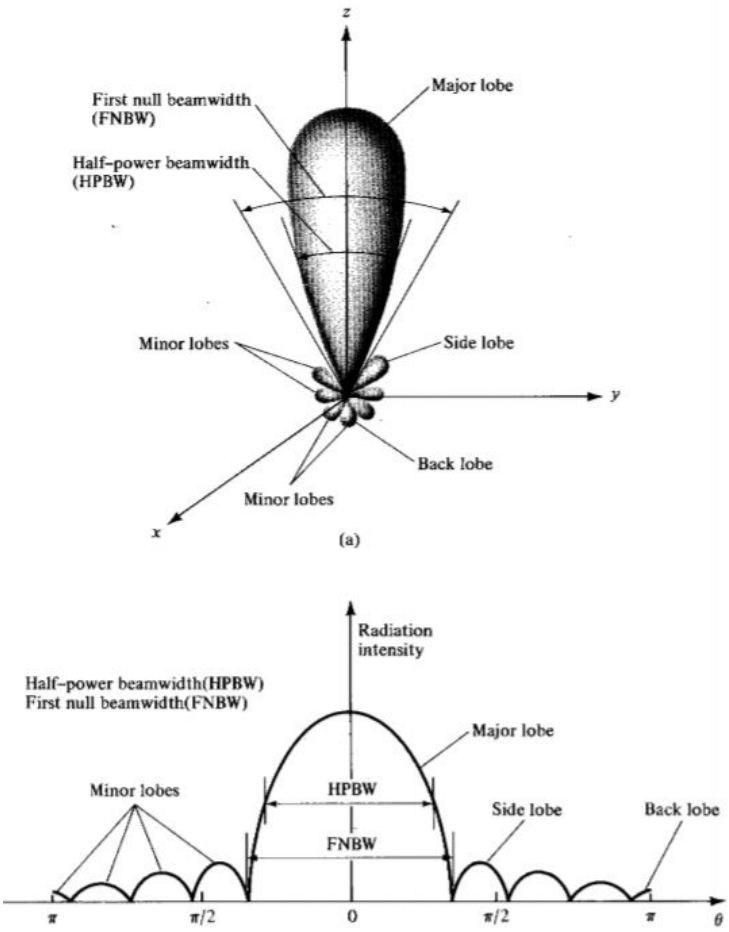

Figure 3: Antenna power pattern. Figure from [1].

2.2 BLACK BODIES, PLANCK AND RAYLEIGH-JEAN LAWS

A black body is an ideal physical body which absorbs and reemits all the electromagnetic radiation isotropically. The black body radiation emitted at thermal equilibrium and at a given temperature follows the Planck's law, shown in equation 4. See Planck's radiation curves at different temperatures as a function of the wavelength in figure 4.

$$B(\nu, T) = \frac{2h\nu^3}{c^2} \frac{1}{e^{\frac{h\nu}{K_B T}} - 1} \tag{4}$$

where $B(\nu, T)$ is the spectral brightness [W . m^{-2} . sr^{-1} . Hz^{-1}], ν is the frequency [Hz], h is the Planck's constant [$6.63x10^{-34}$ J.s], K_B is the Boltzmann constant

$[1.38x10^{-23}J.K^{-1}]$ and T is the temperature of the black body [K].

The spectral brightness at temperature T [K], considering microwave wavelengths and ordinary surface temperatures meets $hv << K_Bt$ conditions, and then it is possible to apply approximation 5:

$$B = \frac{2K_BT}{\lambda^2} \tag{5}$$

where K_B is the Boltzmann's constant and λ is the wavelength.

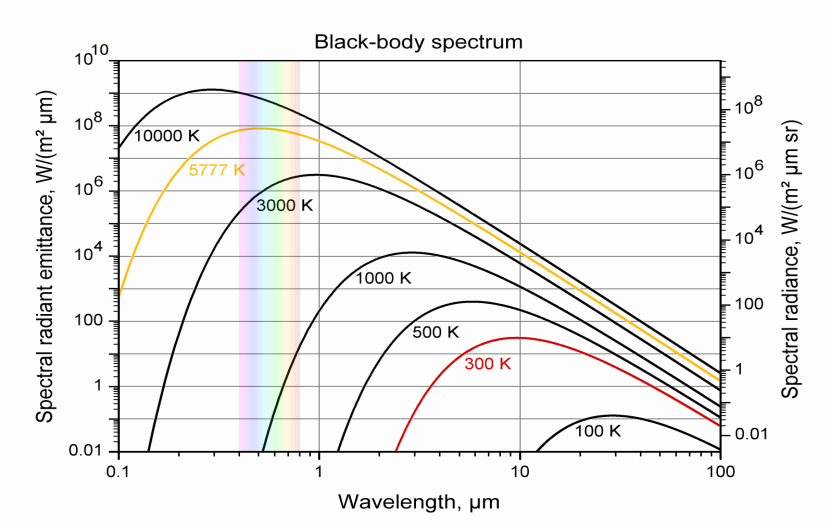

Figure 4: Blackbody radiation curves: Brightness spectral density as a function of wavelength for different temperatures. Figure obtained from [7].

Figure 5 compares the Planck and Rayleigh-Jean laws at a temperature of 300 K. It demonstrates that both laws are the same when $hv << K_Bt$. Meanwhile, Planck's law can be approximated by Wien law when Rayleigh-Jeans is not accurate.

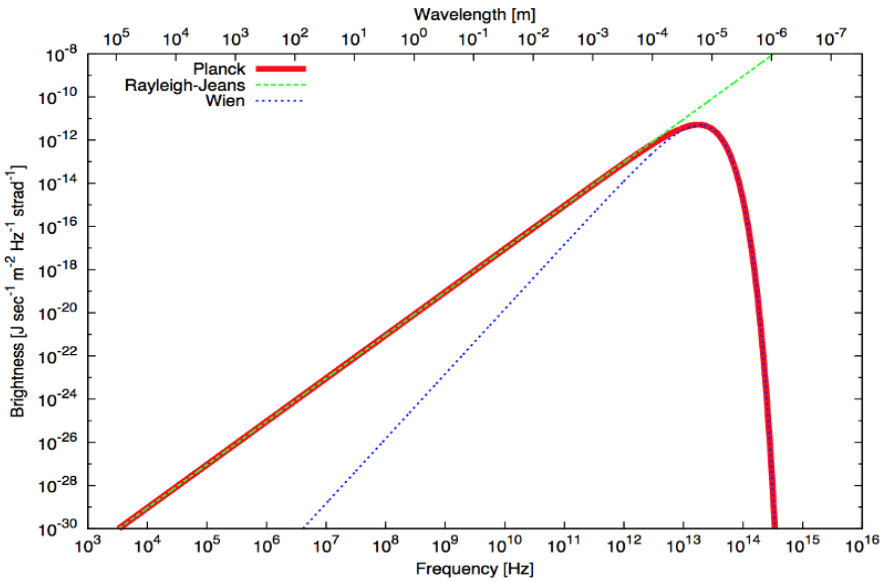

Figure 5: Comparison of Planck's, Wien and Rayleigh-Jean laws at T=300K.

Given so, considering a black body with physical temperature T and bandwidth Δf, its brightness follows the equation:

$$B_{blackbody} = \frac{2K_B T}{\lambda^2}\Delta f \tag{6}$$

With this approximation, the equation 3 would be equivalent to:

$$P_{blackbody} = K_B T \Delta f \tag{7}$$

As it can be seen, this expression considers a linear dependence between temperature and power received, that is why it is very important in remote sensing applications.

2.3 GRAY BODIES

Real bodies absorb part of the energy received and reflect the rest directionally. This bodies are called gray bodies.

A new concept appears in the definition of a gray body spectral brightness: the Brightness Temperature (TB).
It is defined as the physical temperature of an ideal black body that emits the same

radiation diagram and spectrum as the gray body (see equation 8). In fact, TB is related to the physical temperature T at which the body is by its emissivity (e):

$$TB = \frac{B'\lambda^2}{K_B} \tag{8}$$

$$TB = eT = (1 - \Gamma)T \tag{9}$$

where e is the emissivity of the body (1 for a blackbody and e<1 for a gray body), and Γ is the reflectivity of the body.

Then, the spectral brightness for a gray body is defined as follows:

$$B_{greybody} = \frac{2K_B}{\lambda^2}.TB.\Delta f \tag{10}$$

2.4 L-BAND EMISSION OF LAND SURFACE

The passive microwave soil moisture retrieval characterises the body emission, and so the soil moisture, using the temperature brightness TB.

The TB of an object is determined by the physical temperature T and its emissivity e, and e depends on the material dielectric constant ϵ, which at the same time depends on water content. The dielectric constant ϵ of the dry soil (3.5) and the water (80) at microwave frequencies is exceptionally different. This causes a fluctuation of the soil dielectric constant in a range from 4 to 40, depending on its water content.

There are other factors that also influence the TB: vegetation cover, soil surface roughness, soil and vegetation temperature, among others. Depending on the characteristics of the soil, the TB will be approximated differently.

Sections 2.4.3, 2.4.4 and 2.4.5 explain how each of these factors influence the TB.

2.4.1 *Water content*

Water content is the quantity of water contained in the soil.

It can be defined in two different ways:

1. Gravimetric water content (θ_g) is the mass of water per mass of dry soil in a given sample. In order to measure it, it is necessary to weight a soil sample (m_{wet}), then dry it to eliminate the water contained in the sample, and weight it again (m_{dry}).

$$\theta_g = \frac{m_{water}}{m_{soil}} = \frac{m_{wet} - m_{dry}}{m_{dry}} \tag{11}$$

2. Volumetric water content (θ_v) is the volume of liquid water per volume of soil.

$$\theta_v = \frac{Volume_{water}}{Volume_{wet}} = \frac{Volume_{water}}{Volume_{soil} + Volume_{water} + Volume_{air}} \tag{12}$$

where $Volume_{water}$ is the volume of water and $Volume_{wet}$ is the sum of the total wet material volume, including the solid material, water and air.

2.4.2 *Thermal radiation and surface emissivity*

The Earth surface thermal radiation can be described by Rayleigh-Jeans law (equation 5) given microwave wavelengths and ordinary surface temperatures.

The emissivity of a surface can be obtained from the reflectivity, following Kirchoffs reciprocity theorem:

$$e_p = 1 - \Gamma_p \tag{13}$$

where e_p and Γ_p are the emissivity and reflectivity of the rough surface for a polarization p.

The reflectivity of vertical and horizontal polarizations for a smooth surface with a uniform dielectric constant follows the equation 14 [43].

$$\Gamma_h(\theta) = |\frac{cos\theta - \sqrt{\epsilon - sin\theta^2}}{cos\theta + \sqrt{\epsilon - sin\theta^2}}|^2 \Gamma_v(\theta) = |\frac{\epsilon.cos\theta - \sqrt{\epsilon - sin\theta^2}}{\epsilon.cos\theta + \sqrt{\epsilon - sin\theta^2}}|^2 \tag{14}$$

where $\Gamma_{h(\theta)}$ and $\Gamma_{v(\theta)}$ are the horizontal and vertical polarization reflectivity of the smooth surface respectively, ϵ is the dielectric constant (permitivity) and θ is the view angle measured from the normal to the surface.

2.4.3 *Soil dielectric constant*

The dielectric permittivity (ϵ) of the soil measures is its ability to hold an electrical charge).

$$\epsilon = \epsilon' + j\epsilon'' \tag{15}$$

ϵ', the real part, is called the dielectric constant and represents the ability of the material to store electric energy. ϵ'', the imaginary part, is called the loss factor and represents the loss of electric energy in the material.

This soil dielectric constant depends strongly on the water content, but also on other factors such as the soil texture, the temperature or the frequency.

Several papers studied the soil dielectric constant fluctuation at microwave frequencies (James R. Wang and T. Schmugge, 1980 [38]; Eni G. Njokul and Dara Entekhabi, 1994 [34]).

It has been observed that the dielectric constant increases slowly with the water content up to a certain transition point. Once the point is reached, the dielectric constant increases much faster with the soil moisture.
The transition point depends on the characteristics of the soil (or soil texture), being higher for high clay content soils than for sandy soils. This soil type effect on the transition point depends on the frequency: it is weak for frequencies < 1 GHz and strong for frequencies > 1 GHz. See figure 7, showing the transition points for different types of soil at a frequency of 1.4Ghz, 1.42GHz and 5GHz.

Frequency is also a factor that influences the dielectric constant. See in figure 6 how the real and imaginary part are affected. For frequencies below 5 GHz, the real part is weakly frequency dependent. Regarding the imaginary part, it changes with the frequency, which means that the radiation loss through the medium is frequency dependent. In addition it is seen the moisture dependence. Another interesting variable is the penetration depth, which allows to measure at which depth the electromagnetic radiation falls to I/e due to the attenuation loss (see equation 16).

$$\delta = \frac{\lambda}{4\pi n''} \tag{16}$$

where, n'' is the imaginary part of the refractive index, n = $\sqrt{\epsilon}$ and ϵ the dielectric constant.

For both dry and wet soils, the dielectric constant depends very weakly on the temperature, for the ordinary temperature range in the nature. However, frozen soils have very low dielectric constant due to the solid dry state (P. Hoekstra A. Delaney, 1974 [20]).

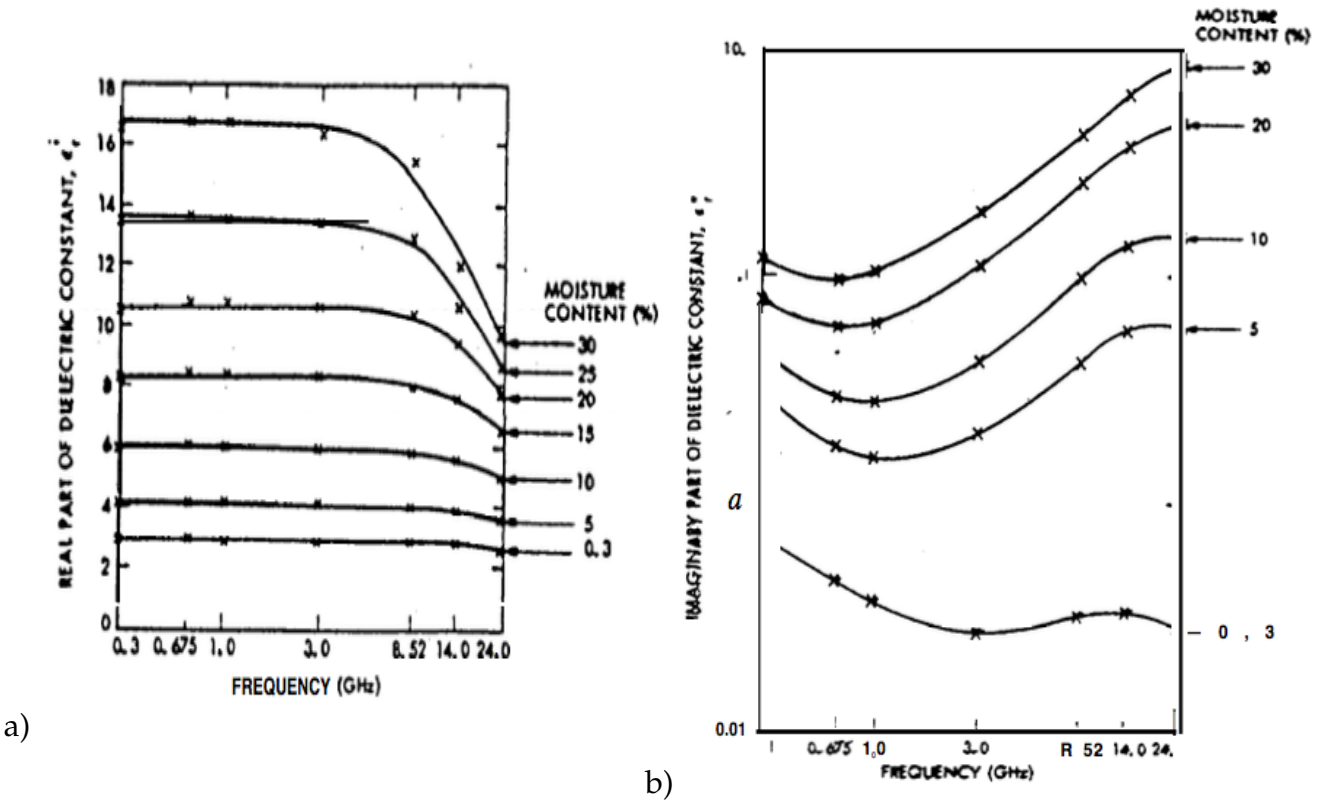

Figure 6: a) and b) show how real and imaginary parts from the dielectric constant depend on the frequency at different moisture content. Figures obtained from [34]

a)

No.	Soil Type	Texture (%)			Wilting* Point, WP cm³/cm³	Transition' Moisture, Wt cm³/cm³	Salinity,' S PPT	Remarks
		Sand	Silt	Clay				
1	M5	88.0	7.3	4.7	0.034	0.110	0	Measurement Frequency = 5 GHz (Wang et. al., 1978)
2	F2	56.0	26.7	17.3	0.115	0.150	0	
3	H7	19.3	46.0	34.7	0.220	0.230	3	
4	Harlingen Clay	2.0	37.0	61.0	0.358	0.270	0	
5	Yuma Sand	100.0	0	0	0.004	0.090	0	Measurement Frequency = 1.412 GHz (Lundien, 1971)
2	Eufaula Fine Sand	90.0	7.0	3.0	0.024	0.100	0	
3	Dougherty Fine Sand	82.0	14.0	4.0	0.034	0.100	0	
4	Minco Very Fine Sand	70.0	22.0	8.0	0.051	0.100	0	
5	Openwood Street Silt	22.0	70.0	8.0	0.092	0.150	2	
6	Chickasha Loam	58.0	28.0	14.0	0.098	0.150	2	
7	Zaneis Loam	48.0	36.0	16.0	0.114	0.160	2	
8	Collinville Loam	45.0	39.0	16.0	0.115	0.170	2	
9	Kirkland Silt Loam	26.0	56.0	18.0	0.137	0.150	2	
10	Tabler Silt Loam	22.0	56.0	22.0	0.159	0.140	2	
11	Vernon Clay Loam	16.0	56.0	28.0	0.192	0.180	7	
12	Long Lake Clay	6.0	54.0	40.0	0.255	0.220	9	
1	Sand	86.0	7.0	7.0	0.046	0.14	0	Measurement Frequency = 1.4 GHz (Newton, 1977)
2	Samples 4 and 5	40.0	26.0	34.0	0.205	0.26	9	
3	Samples 7 and 18	36.0	29.0	35.0	0.212	0.23	6	
4	Samples 14 and 15	52.0	9.0	39.0	0.221	0.26	8	
5	Sample 13	44.0	12.0	44.0	0.250	0.27	9	
6	Miller Clay	3.0	35.0	62.0	0.361	0.30	10	

b)

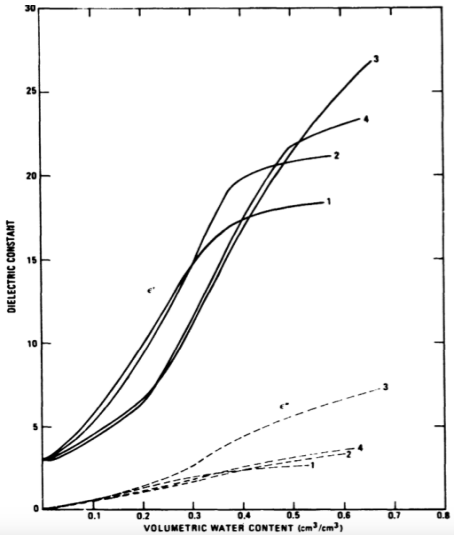

c)

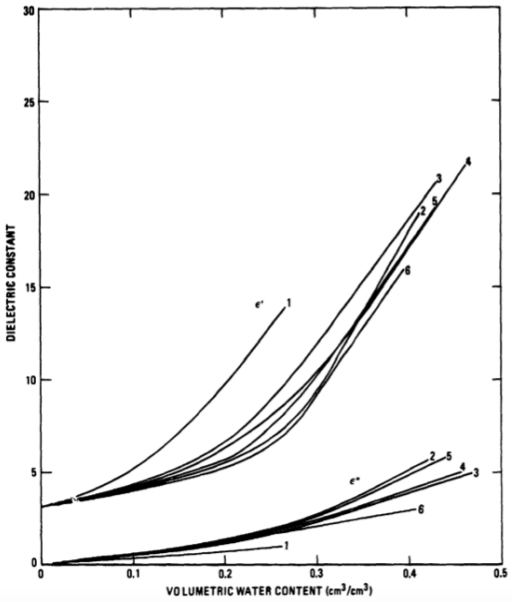

d)

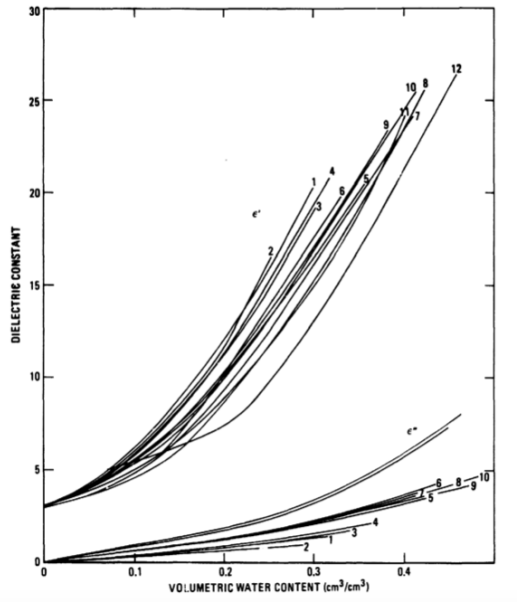

Figure 7: The dielectric constants versus volumetric water content for 4 soils at 5 GHz, 6 soils at 1.4 GHz and 12 soils at 1.42 GHz are presented in b), c) and d) respectively. Soils characteristics are listed in a). Figures obtained from [38]

2.4.4 *Surface roughness*

The emissivity of a rough surface can be obtained from the reflectivity, following Kirchoffs reciprocity theorem (equation 13).

The reflectivity of vertical and horizontal polarizations for a flat surface with a uniform dielectric constant follows the equation 14.

In the case of rough surfaces, a correction needs to be applied to the reflectivity equations to take into account the effects of surface scattering (Xinming et al., 2010 [43]).

$$\Gamma(\theta,\phi) = \frac{1}{4\pi}\int\int_{2\pi}[\gamma_{pp}(\theta,\phi;\theta',\phi') + \gamma_{pq}(\theta,\phi;\theta',\phi')]d\Omega \tag{17}$$

in which p and q refer to the vertical and horizontal polarizations.

There is some literature on how to work with this expression (e.g. Fung and Eom, 1981 [16]; Tsang and Newton, 1982 [33]), but the methods described are complex. Instead, a simpler semi-empirical model has been developed (Wang and Choudhury, 1981 [37]; Wang et al., 1983) in order to easily calculate the reflectivity (see equation 18):

$$\Gamma_{sp}(\theta) = [(1-Q_s)\Gamma op(\theta) + Q_s\Gamma_{op}(\theta)]e^{-h_s cos(\theta)^n} \tag{18}$$

when $h_s = 4k^2\sigma_s^2$

where Γop is the reflectivity at vertical or horizontal polarization of a smooth surface (equation 14), h_s is the soil roughness parameter (dependent on k and σ_s, the electromagnetic wavenumber and standard deviation of surface height, respectively) and θ is the angle of incidence measured from the normal to the surface.Q_s is the polarization mixing parameter and n models the angular dependency of the roughness.

Wigneon et al. in [39] established that for L-band, Q_s and n could be considered 0 and h_s could be calculated semi-empirically.

Figure 8 shows the roughness surface effect on the brightness temperature. It displays the brightness temperature as a function of the incidence angle at three different frequencies for two surfaces (smooth and rough). It can be seen that for rough surfaces, the brightness temperature increases and the difference between the vertical and horizontal polarizations is reduced.

When the surface roughness increases, the sensitivity of brightness temperature to soil moisture decreases. Therefore, it is necessary to apply corrections to calculate soil moisture accurately. Nevertheless, in many cases, the surface roughness is small enough to be corrected by doing estimates of the roughness parameters.

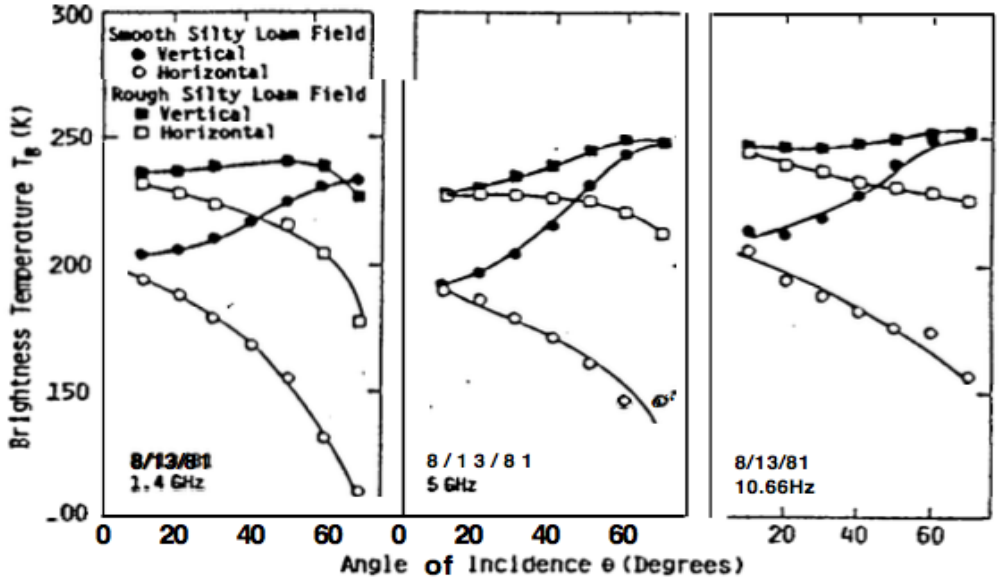

Figure 8: *TB* vs roughness. Vertical polarizations represented by line with black dots and the horizontal one with lines of white dots. Figure obtained from [34].

2.4.5 *Vegetation effect*

Vegetation absorbs, reflects and scatters microwave radiation. Also, it can even contribute by emitting its own energy. The vegetation is modeled as a layer on top of the soil. The effect of the vegetation in the passive microwave soil moisture retrieval has been studied and modeled in the literature (Zheng Xingming et al., 2014 [42]; Eni G. Njokul and Dara Entekhabi, 1994 [34]; Mina Moradizadeh et al., 2016 [31]; Zhiqiang Gaoa et al., 2011 [44]; Jackson, T. J et al, 1991 [27]; Jackson, T. J. et al., 1972 [28]; Kirdiashev, K. P. et al., 1979 [29]).
The brightness temperature model that takes into account vegetation cover effect, is summarized in equation:

$$TB_p = e_p T_e \gamma + T_c(1-\gamma)(1-\omega) + T_c(1-e_p)(1-\omega)(1-\gamma)\gamma \tag{19}$$

p stands for the polarization, T_e is the soil effective temperature, T_c is the vegetation temperature, γ is the vegetation layer transmissity, ω is the single scattering albedo and e_p the emissivity of the soil surface.
ω depends on the geometry since it affects radiative transfer in a scattering medium. γ can be defined as a function of the vegetation opacity and the incidence angles $\gamma = e^{\frac{-\tau}{cos\theta}}$.

τ can be related linearly to the log of the NDVI in the following way (Burke et al. [19]):

$$TB_p = \alpha + \beta(1 - log(NDVI)) \tag{20}$$

For low vegetation (small τ) $TB_p \simeq e_p T_e$ (brightness temperature is very similar to the soil brightness temperature), while for dense vegetation (high τ) $TB_p \simeq T_c$ (brightness temperature tends to the vegetation temperature).

Figure 9 shows the dependence of emissivity on soil moisture when varying the amount of vegetation. It has been calculated using equation 19.

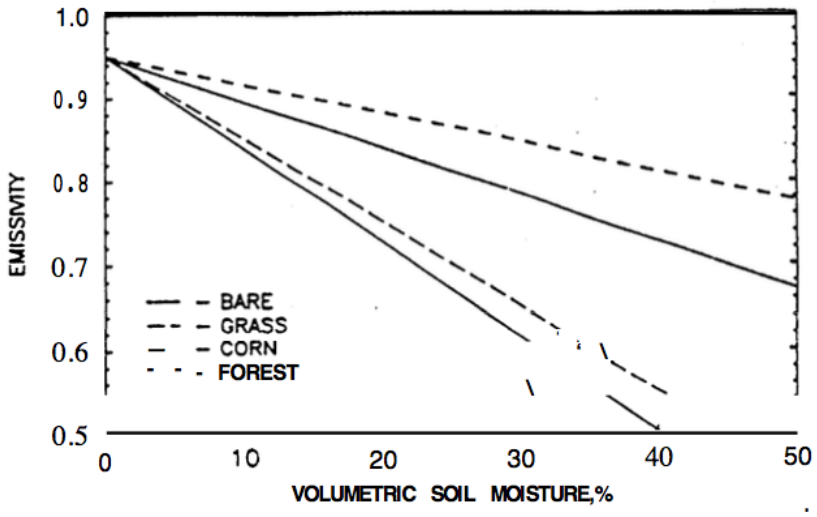

Figure 9: Emissivity vs vegetation. Figure obtained from [34].

3

RELATIVE SOIL MOISTURE EXTRACTION: MISSIONS

3.1 EUROPEAN SPACE AGENCY (ESA)

European Space Agency or ESA [4] is an intergovernmental organization founded in 1975 including 22 member countries with the aim of promoting cooperation among European States in Space exploration by managing their monetary and intelectual resources to achieve better results than a single European state alone would obtain. It recommends common objectives and industrial policies, implements activities in the Space research field and integrates national projects into the European program.

The current members states of ESA are: Austria, Belgium, Czech Republic, Denmark, Estonia, Finland, France, Germany, Greece, Hungary, Ireland, Italy, Luxembourg, Netherlands, Norway, Poland, Portugal, Romania, Spain, Sweden, Switzerland, United Kingdom.

ESA is currently developing different project, such as, Horizon 2000, Cosmic Vission (successor of Horizon 2000), Living Planet Programme, Copernicus Programme, Exomars and Galileo.

3.2 SOIL MOISTURE AND OCEAN SALINITY SATELLITE (SMOS)

SMOS [12] is a satellite launched by ESA as part of the "Living Planet" Programme in 2009.
SMOS mission was intended to last at least three years, extensible to 5. But, given its good results it has been working for 9 years already and at this moment, the mission has been even extended to 2021.
SMOS is basically a spacecraft platform (Proteus) with the single payload, the radiometer MIRAS (Microwave Imaging Radiometer using Aperture Synthesis). SMOS

describes a circular polar orbit at altitude 758 km and works in the protected L-band (21 cm-1.4 GHz).

3.2.1 *SMOS mission objectives and data requirements*

SMOS main objectives are:

1. Globally monitor surface soil moisture over land surfaces.
   Soil moisture is the quantity of water within a given volume of a material, often represented as a percentage.
   It is regulated by rain and evaporation processes and it strongly influences water and heat flux between the land and the atmosphere, which is essential in climate and weather. High soil moisture causes an important increment of atmosphere humidity and the lowering of the temperature locally.
   Soil moisture data can be used to improve short and medium term weather forecasting, build hydrological models, predict climate disasters and monitor the plant growth.

2. Globally monitor surface salinity over the oceans.
   The ocean plays an important role in the climate system.
   Salinity, quantity of salt per unit volume expressed in psu (practical salinity units), is one of the important factors that determine the ocean thermohaline circulation, jointly with the water and heat flux between the athmosphere and the ocean. Ocean surface density increases when salinity and temperature raise. When water evaporates, the salt concentration increases and the surface layer becomes denser. On the other hand, the rain causes a density reduction in the surface water layer. Freezing and melting of seawater also affect the salinity.
   When the density in the surface layer of the seawater is high enough, the denser water sinks. So, thermohaline circulation continually replaces deep seawater with salty water from the surface and slowly replaces the layer of surface water with water from deeper depths. This ocean circulation is vital in the regulation of climate and weather.
   Finally, salinity also plays a role in the oceanic carbon cycle, regulating the CO_2. The use of sea surface salinity assimilation measurements could help to estimate the absorption of CO_2 by the ocean.

3. Improve the modelization of surfaces covered by snow and ice.
   The greenhouse effect can be tracked and predicted by using observations of the ice caps extension in the sea. Sea level rise is also related to climate change, and widely depends on the ice sheets. Finally, the snow extension influences the hydrological

Data product	Requirements
Soil moisture	Accuracy:4% Spatial resolution:35-50 km Time resolution: 1-3 days
Salinity	Single observation: Accuracy: 0.5-1.5 psu Global observation: Accuracy: 0.1 psu Spatial resolution: 200 km Time resolution: 10-30 days)

Table 1: SMOS requirements

and climatological course. Also, it is an indicator of the climate change since the climate warning causes that the surface covered by snow moves northwards in the Northern hemisphere.

The measurement requirements for soil moisture are listed in table 1: an accuracy of 4% volumetric soil moisture, spatial resolution of 35-50 km and a periodicity of 1-3 days. For salinity, SMOS is intended to provide data with accuracy of 0.5-1.5 psu for a single observation and accuracy of 0.1 psu for an ocean area of 200 x 200 km averaging 10-30 days. As secondary goal, SMOS is also meant to acquire maps with vegetation water content (VWC) data with a periodicity of 6 days.

3.2.2 *MIRAS instrument*

MIRAS (Microwave Imaging Radiometer using Aperture Synthesis) is a 2D interferometric radiometer that works in L-Band (21 cm-1.4 GHz).
It is the only payload of the SMOS mission and it is the first interpherometric radiometer put in orbit.

MIRAS has 3 arms divided in three segments and a central structure. Figure 10 shows an image that simulates SMOS in orbit.

Figure 10: Artist view of SMOS mission (Y shape, solar panels and Protheus platform). Figure from [5].

A huge antenna, approximately of 10 meters of diameter, would be necessary to meet the spatial resolution requirements for soil moisture and salinity data acquisition in L-band. At that time, it was technologically impossible to send to the space an antenna of such dimensions.

SMOS overcomes this challenge by using instead of such huge antenna an array of 69 antenna-receiver integrated elements, called LICEF, equally distributed over 3 arms and hub. A LICEF (LIght and Cost Effective Front-end) is a unit composed of an antenna-receiver that measures the L-Band radiation conveyed by the Earth. The spatial resolution is acquired by sending the signals collected in each LICEF to a central correlation unit, that computes the complex cross-correlation between each combination of signal pairs (see 11). The objective is to measure the phase difference of the radiation obtained by the different small receivers.
There is a data preprocessing step on board, which reduces the quantity of data to be transmitted to the ground.

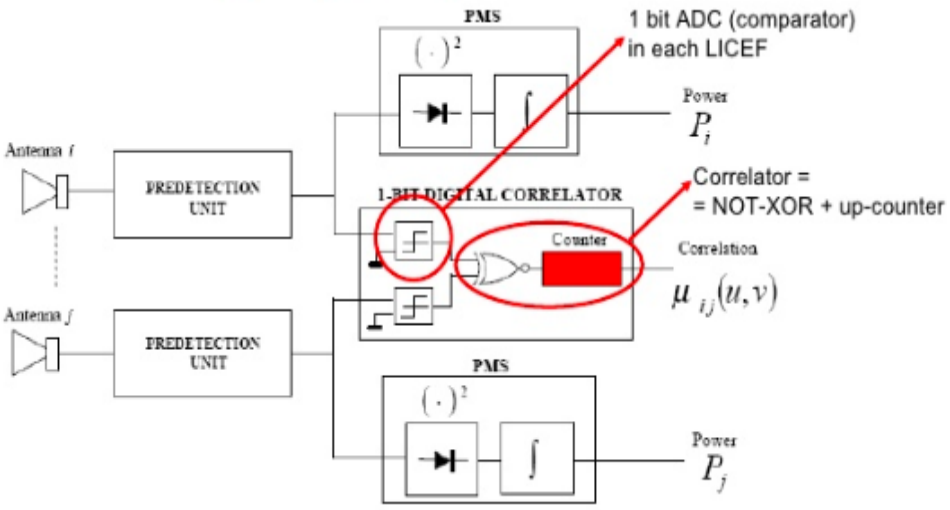

Figure 11: Digital Correlator System (DICOS)

3.2.3 *Data products*

SMOS data products are divided in 4 different levels based on their processing degree:

- Raw Data: It is the payload data obtained directly from the satellite, without any processing applied. The data includes observations and telemetry in its original format (CCSDS packets).

- Level-0 products: The payload data is added to Source Packets with Earth Explorer header. They are reconstructed chronologically and almost no processing is applied to the data: duplicated packets are eliminated and they are separated in ascending/descending measurements.

- Level-1 products are classified in three subgroups:

  - L1A products: It contains snapshots of the observations and telemetry data reformated and calibrated, which means that internal calibrations have been used to correct the correlations. The data is still chronologically ordered.

  - L1B products: The image reconstruction process is deployed. The input data is transformed into Fourier components of brightness temperatures referenced to the antenna polarisation frame. Also, many corrections are applied in order to eliminate interferences (galactic background, sun and moon).

  - L1C products: There are available two different product types, one for land data and another for sea data.
    The inverse fourier transform is applied in order to obtain the brightness temperatures in the real domain again, which are geolocated by assigning latitude and longitude values in a predefined grid. Each grid point contains multi-angular brightness temperature values.

- Level-2 products for soil moisture and salinity are computed from L1c product brightness temperatures. The calculation of L2 from L1c implies a correction step, in order to mitigate atmospherics's phenomena such as the Faraday effect and the attenuations and interferences from the sun, the moon or the Galaxy.

- Level-3 data is obtained from level-2 product by interpolating to a 25km grid. Before the interpolation, a filtering process is applied with the objective of eliminating low quality values, negative humidity values and pixels with a high radio frequency interference (RFI) probability.

- Level-4 products are obtained using synergies with L3 data and data from other satellites or models, such as land surface temperature and vegetation index. They are used for example to improve the the spatial resolution from 30km to 1km.

3.3 AQUA AND TERRA MISSIONS

Aqua and Terra missions are included in the NASA's ESE (Earth Science Enterprise) program.
MODIS instrument on board of both Terra and Aqua missions obtain Land Surface Temperature (LST) and Normalized Difference Vegetation Index (NDVI) information. They obtain images of the same area on Earth approximately three hours apart and work in tandem to achieve global Earth coverage in less than 1 day.

3.3.1 *Aqua mission*

Aqua was launched in May 4 of 2002, from Vandenberg Air Force Base. EOS/PM-1 was its initial name, according to the time it crosses the equator.
This mission was intended to last 6 years, but this project has already been active almost 17 years.
It follows a sun-synchronous orbit at 705km of altitude, crossing the equator daily at 1:30 P.M. local time from south to north (ascending node).

The data provided by this satellite gives information of cloud formation, rain, radiation, Energy Cycle, Carbon cycle and moisture.

Aqua carries six instruments, which acquire different data:

- Atmospheric Infrared Sounder (AIRS): It is focused in climate research and weather forecasting by obtaining air and surface temperature, cloud formations, and atmospheric humidity.

- Advanced Microwave Sounding Unit (AMSU-A): It is meant to obtain temperature and humidity profiles. It included 15 channels (from 15 to 90 GHz) but currently 5 of them are down.

- Humidity Sounder for Brazil (HSB): It provides humidity measures by using 4 channels (between 120 and 183 GHz) even in highly unfavorable cloud conditions.

- Advanced Microwave Scanning Radiometer for EOS (AMSR-E): It measures winds and temperature in the sea surface, cloud formations, radiative energy flux, ice and snow.

- Clouds and the Earth's Radiant Energy System (CERES): It measures the athmosphere radiant energy , jointly with the UV radiation reflexed and absorved by the surface, clouds and the athmosphere. It was luanched with three channels but currently only two of them are operational (band between 0.3 and 5 microns and between 8 and 12 microns).

- Moderate-Resolution Imaging Spectroradiometer (MODIS): It measures radiative energy cycle, cloud formations, land cover, fires and volcanoes.

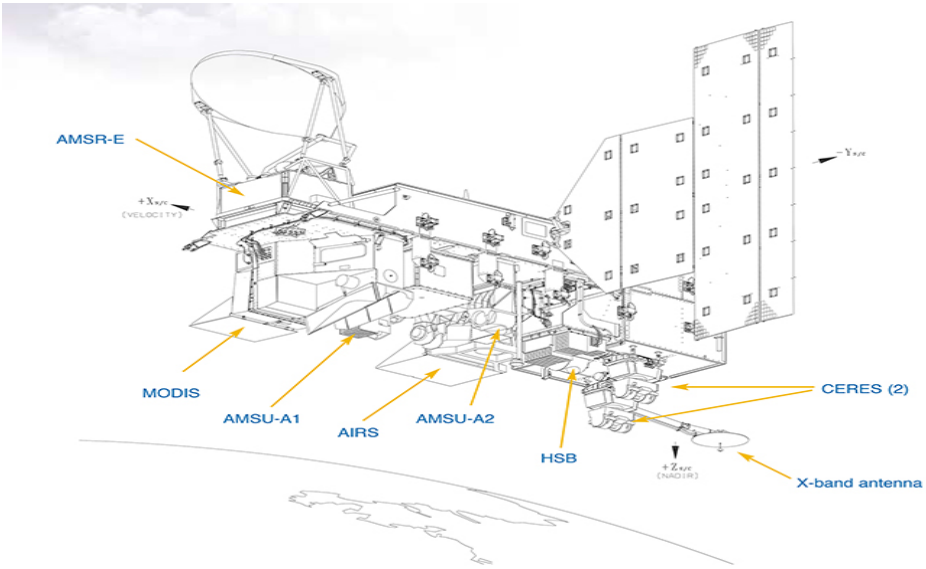

Figure 12: Aqua spacecraft instruments. Figure obtained from [2].

3.3.2 *Terra mission*

Terra was launched in December 18 of 1999 from Vandenberg Air Force Base by NASA. Its former name was EOS AM-1 since its orbit passed over the equator at 1 in the morning. It was initially planned to last 6 years, but it has been extended and it is still working.

It has a sun-synchronous orbit at 705 km above Earth's surface.

Currently, the Terra satellite equator crossing time is at 10:30-10:45 a.m. local time from North to south (descending orbit).

It carries five different instruments:

- Advanced Spaceborn Thermal Emission and Reflection Radiometer (ASTER): It is composed of three sensor subsystems working at different spectral regions: Short-wave Infrared (SWIR), no longer available, Visible and Near Infrared (VNIR) and the Thermal Infrared (TIR). It provides high-resolution images of land surface, cloud formations, water and ice.

- Clouds and the Earth's Radiant Energy System (CERES): Explained in Aqua mission section.

- Multi-angle Imaging Spectroradiometer (MISR): It provides images of the Earth from cameras pointing at nine different angles. It monitors aerosol particles in the atmosphere, characteristics and types of clouds and land surface cover.

- Measurements of Pollution in the Troposphere (MOPITT).

- Moderate-resolution Imaging Spectroradiometer (MODIS).

3.3.3 *MODIS*

The MODIS instrument works in 36 spectral bands (wavelength from 0.4 μm to 14.4 μm). Two bands are imaged at a nominal resolution of 250 m at nadir, with five bands at 500 m, and the remaining 29 bands at 1 km. A 55-degree scanning pattern at the EOS orbit of 705 km achieves a 2,330-km swath and provides global coverage every one to two days (see table 2).

Orbit	705 km sun-synchronous near-polar circular
Equator crossing time	Terra (descending node): 10:30 a.m Aqua (ascending node): 13:30 p.m
Spatial resolution	250 m (bands 1-2) 500 m (bands 3-7) 1 km (bands 8-36)
Time resolution	1-2 days

Table 2: MODIS characteristics

The original downscaling product distributed at BEC used the MOD13A2 MODIS product as NDVI and MYD11A1 as Land Surface Temperature (LST), both at 1km resolution. LST is provided daily and NDVI in a 16-days product.

3.4 SENTINEL PROGRAMME

ESA is currently developing Earth observation missions under the Copernicus Programme framework. Sentinel Programme Earth observation missions includes radar and super-spectral imaging for land, ocean and atmospheric monitoring. Figure 14

shows an artist view of the seven Sentinel satellites.

Currently there are six Sentinel missions:
- Sentinel 1 employs RADAR antennas for the study of land and oceanic surfaces. Since the data RADAR is not affected by atmospheric conditions or the day or night the monitoring is continued. - Sentinel 2 uses MSI (Multispectral Instrument) to obtain high resolution space data and monitorize the terrestrial surface. Among others, it provides images of vegetation, soil and water cover. It includes 13 bands with different spatial resolution (see table 13)

Banda	λ [μm]	Píxel	Banda	λ [μm]	Píxel
1	443	60 m	**5**	705	20 m
9	940	60 m	**6**	740	20 m
10	1375	60 m	**7**	783	20 m
2	490	10 m	**8a**	865	20 m
3	560	10 m	**11**	1610	20 m
4	665	10 m	**12**	2190	20 m
8	842	10 m			

Figure 13: Sentinel 2 bands

- Sentinel 3 is a multi-instrument mission to measure sea and land surface temperature, ocean and land surface color with high accuracy. It covers the earth.

- Sentinel 4 and Sentinel 5 will be launched in 2021 with the aim of providing data of trace gases and aerosols concentrations in the atmosphere over the European zone. They will deploy air quality measurements, Ozone concentration monitoring, Solar Radiation measurements and climate monitoring.

- Sentinel 6 will measure the ocean topography over the world.

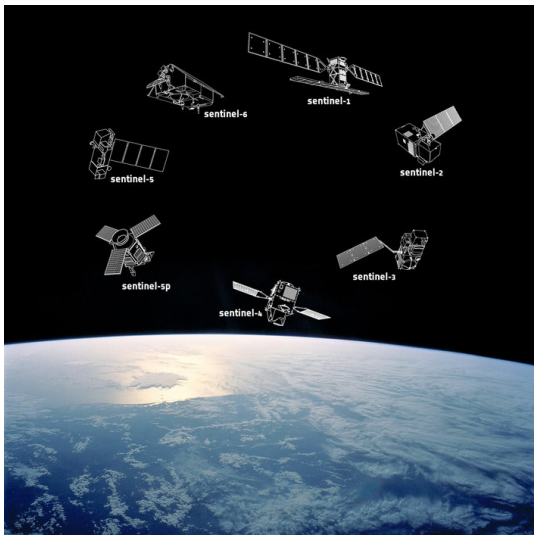

Figure 14: Sentinel family

3.4.1 *Sentinel 3*

Sentinel 3 mission obtains LST and NDVI data using its SLSTR instrument on board.

Sentinel-3 has a sun-synchronous orbit, at an average altitude of 815 km, which crosses the equator with its descending node at 10:00 A.M. mean local solar time.

Sentinel 3 mission is formed by a constellation of two satellites: Sentinel-3A, launched in February 2016, and Sentinel-3B launched in April 2018. Both have the exact same orbit, the difference is that Sentinel-3B is +/-140 degrees phased with Sentinel-3A. This phasing value optimizes global coverage and sampling of ocean currents by the altimeters in Sentinel-3A and -3B.

The orbital cycle, time elapsed between observations of the exact same geographical point on earth, is 27 days, 385 orbits per cycle.

Sentinel-3 carries several instruments:

1. OLCI. It provides serveral product types [9] that can be divided in:

   a) L1-Processing: It gives the radiance for each pixel in the instrument grid, each view and each OLCI channel as well as annotation data.

   b) L2-Processing: It obtains full and low resolution atmospheric and land geophysical data.

2. SLSTR. It provides different product types [10] that can be divided in:
   a) L1B, providing brightness temperature
   b) L2-WST, containing Sea Surface Temperature (SST) measurements following the GHRSST specifications
   c) L2-LST, is the land surface temperature information
   d) L2-WCT, adding Sea Surface Temperature (SST) for single and dual view
3. Synergy [11]. Its products can be classified in:
   a) L2-Syn, providing surface reflectance and aerosol parameters over land.
   b) L2-VGP, containing TOA (Top of athmosphere) reflectances, light reflected off the surface and off the atmosphere.
   c) L2-VGI and V10, vegetation-like products
4. Altimetry [8].
   a) Level1A: geo-located and calibrated bursts of echoes.
   b) Level1B: geo-located, calibrated and processed to reduce the standard deviation of the noise (multi-look) level high resolution power echoes.
   c) Level1B-S: Processed (SAR), calibrated high resolution complex echoes arranged in stacks after slant range correction before multi-look processing.
   d) Level2- WAT: Water products generated by the Marine Centre.
   e) Level2-LAN: Land products built by the Land Centres.

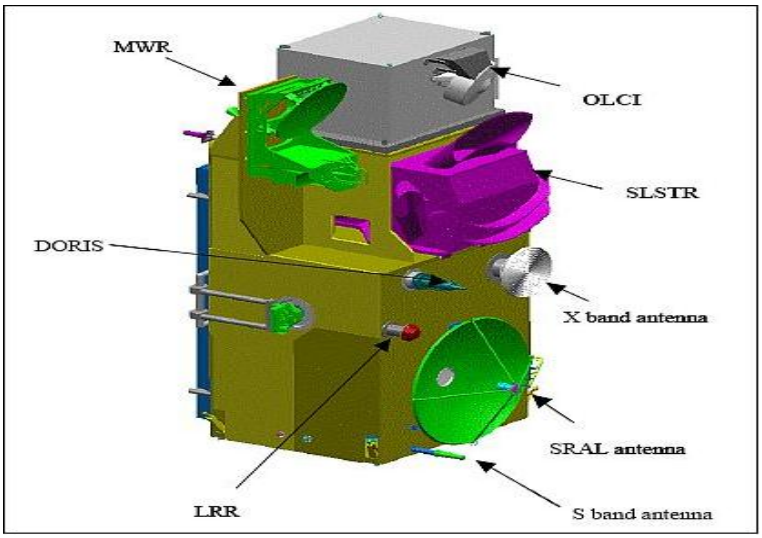

Figure 15: Sentinel-3 spacecraft

In this thesis, we will use L2-LST product obtained from SLSTR, which contains LST information as primary product and NDVI as ancillary data. For this product, global coverage is obtained at the equator every two days with one satellite and in one day with two satellites (see table 3).

	Constellation configuration	Revisit at equator	Revisit for latitude >30	Specification
SLSTR dual view (day and night)	1 satellite	<1.8 days	<1.5 days	<0.4 days
	2 satellites	<0.9 days	<0.8 days	

Table 3: SLSTR dual view revisit time considering only Sentinel-3A and then both Sentinel-3A and Sentinel-3B.

3.4.2 *SLSTR instrument*

SLSTR is the instrument on boeard of Sentinel 3 that provides the L2-LST product that will be used later as ancillary data in the downscaling algorithm to obtain high resolution soil moisture maps.

SLSTR (Sea and Land Surface Temperature Radiometer) is a conical scanning image radiometer that obtains a set of infra-red radiance measurements, from which a wide

range of products are provided: land surface temperature, ice surface temperature, atmospheric aerosol, active fire monitoring, cloud, forestry and hydrology products.

SLSTR is an advanced version of the AATSR instrument on Envisat. Its main purpose is to ensure data continuity of (A)ATSR products, that is why it includes their basic functionality jointly with new features: higher resolution in some channels, wider swath two new channels.

It includes a total of 11 different spectral channels:

- 3 visible channels (VIS) at 0.87, 0.67 and 0.55 micron.
- 3 thermal infra-red channels (TIR) at 3.7, 10.8 and 12 micron wavelengths.
- 3 short wave channels (SWIR) at 2.25, 1.6, 1.375 micron wavelengths.
- 2 fire channels at 3.7, and 10.8 micron wavelengths;

The SLSTR is separated into the Optical Scanning Unit (see figure 16), containing the Optomechanical Enclosure (OME) and Detection Assembly (DA), and then the SLSTR control and processor electronics unit.

Figure 16: SLSTR Optical Scanning Unit. Figure obtained from [14]

An scheme of the structure of SLSTR instrument is presented at figure 17.

SLSTR instrument uses two scan mirrors placed at an oblique angle to its rotation axis. They reflect the radiation into a telescope assembly with its optical axis parallel

to the rotation axis. When the scan mirrors rotate, they generate a cone, from which the Earth view swaths are obtained (see figure 18). The mirrors couple scan at 200 scans per minute.

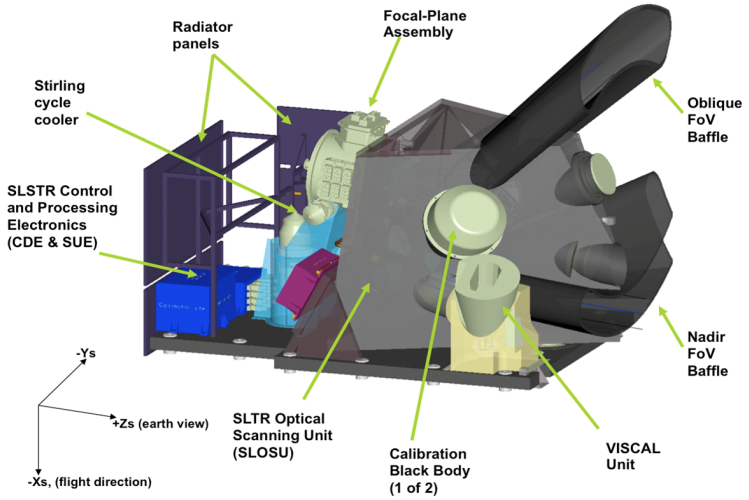

Figure 17: SLSTR structure overview. Figure obtained from [15].

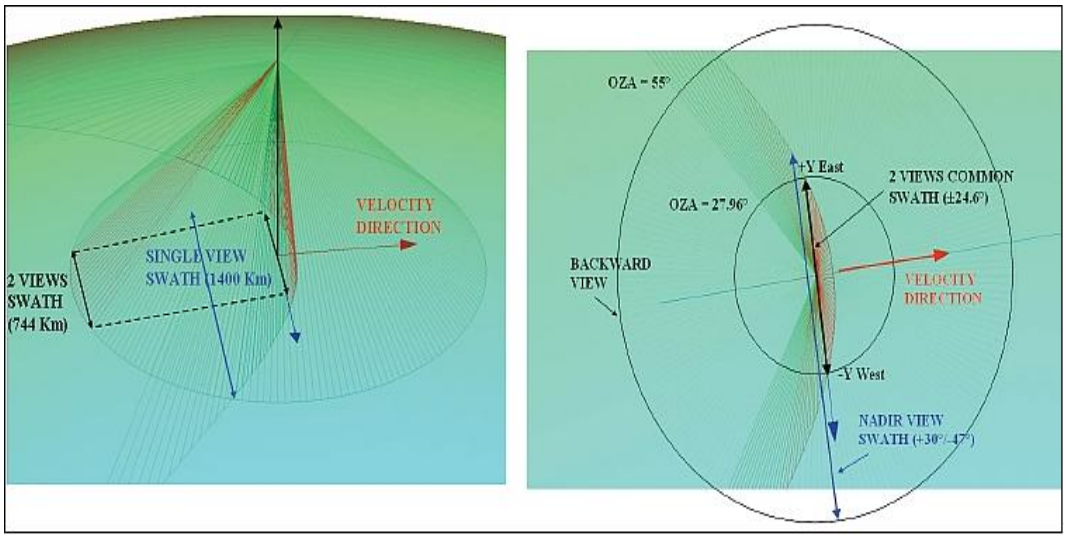

Figure 18: Near nadir (left) and backward inclined (right) views of the scanning mirror geometry of SLSTR instrument on board Sentinel 3.

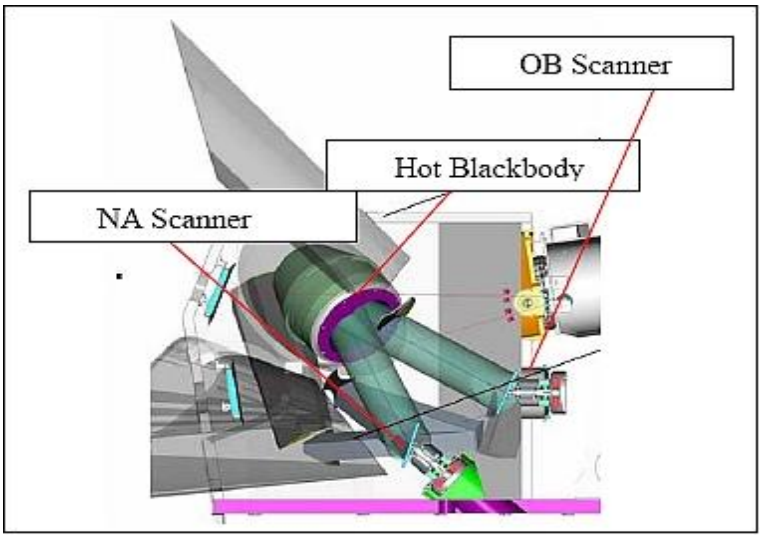

Figure 19: Sectioned SLSTR side-view showing both scanners

3.4.3 *LST and NDVI data from Sentinel 3*

In this project we are interested in Sentinel 3 LST L2 data obtained from SLSTR instrument, which inlcudes LST data as primary product and NDVI as ancillary data. In addition, a cloud mask is provided with the LST L2 product. This mask has been applied at the data preparation process.

It is interesting to highlight that Sentinel 3 provides two different NDVI products: On one hand, a NDVI is provided as ancillary data inside the LST L2 product, which is the one that we will use in this project. It is not a primary product but an ancillary product calculated from the top of athmosphere reflectances. On the other hand, there is the NDVI product provided by Sentinel-3 SYNERGY. This NDVI represents the maximum value composite of ground reflectance measurements of all segments received during one or ten days for the entire surface of the Earth, derived from the B3 and B2 channels. It is a third party product and it is not accessible yet through the hub but it will be in the future.

Summing up, in this project we will use both LST and NDVI data provided inside LST L2 product.

These data can be downloaded for free from Copernicus Data Access Hub [13] in two different ways:

1. Downloading the tiles intersecting the selected geographical area (NRT).

2. Downloading the orbit, which contains the tiles merged, intersecting the selected geographical area (NTC).

The system requirements and methods to process the data will vary depending on data characteristics. In this project we will use NRT due to resources limitation.

Sentinel 3 LST L2 Near-Real-Time (NRT) products download

Data characteristics and availability
Sentinel-3 SLSTR L2 LST Near Real Time (NRT) products are individual tiles. They are uploaded to the dataset hours after its acquisition.
These data products are rolled from the archives after one month. So, only tiles newer than one month before the downloading date are available. After a month, NRT products are replaced by the corresponding Non-Time Critical (NTC) products, which report the data of the whole orbit and are of better data quality than the NRT products.

Each file containing a tile has an approximated size of 60 MB and are in native format .sen3.

The NRT product are useful for obtaining soil moisture maps at 1km resolution from SMOS L3 product at BEC in real time.

NRT files download
NRT products are available from the Pre-Operations Data Hub.

The process to select the data and download it is fast and easy.
The first step is to mark the geographical area of interest. Then, we need to use the filter panel to select the product type, the instrument used to acquire it, the sensing period of time and the timeliness (see figure 20).

The specific product we will use is the Land Surface Temperature, which is a Level-2 product, and it is obtained using the SLSTR instrument. Regarding the timeliness, in order to download the tiles we need to select ”Near Real Time” option.

After the process described above the tiles corresponding to the filtering options we selected are displayed ready to download (see figure 21).

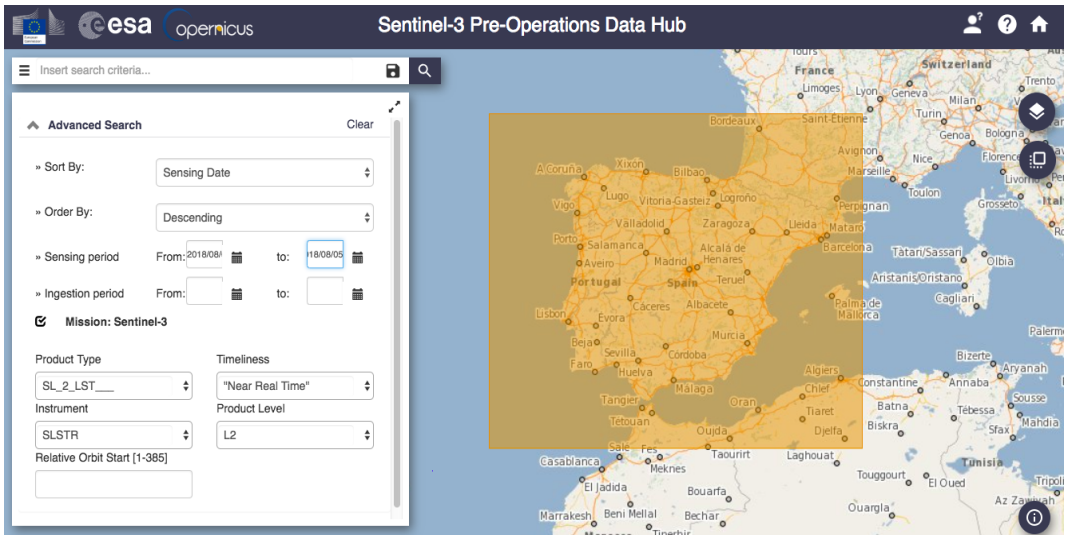

Figure 20: Sentinel 3 product and data acquisition.

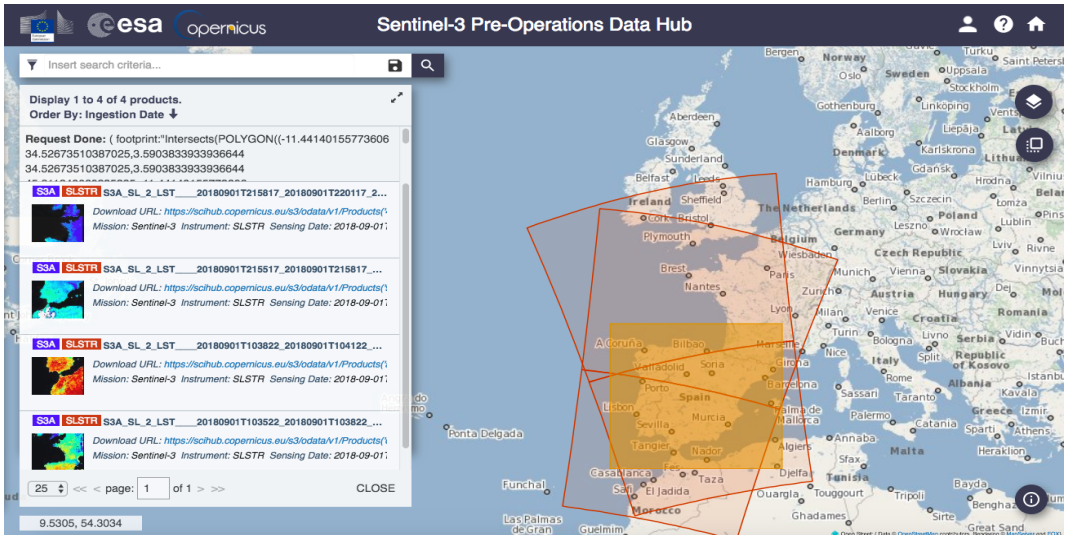

Figure 21: Sentinel 3 LST product tiles

Preparation of the Sentinel 3 LST and NDVI data from NRT product
Once the Sentinel 3 LST L2 tiles are downloaded (see figure 21), it is necessary to combine the LST data and NDVI data in order to obtain a complete image of our area of interest.
After that, the first step is to rewrite the data into NETCDF format, which can be read by Matlab. SNAP (Sentinels Application Platform) is the tool used with this purpose (see figure 22). It is an open source platform containing all ESA's Toolboxes available for the user to process and exploit Earth Observation Data obtained from Sentinel

missions.
Once the LST and NDVI tiles are in the appropriate format, they are merged using Matlab.

The cloud mask is applied to each original file before merging it. The specific cloud mask we use is the probabilistic one.

Figure 23 shows an example of LST tiles merging. The original tiles are presented at figures 23a and 23b and the final result is shown in 23c, when joining them over the Iberian Peninsula.

Figure 24 shows an example of NDVI tiles merging. The original tiles are presented at figures 24a and 24b and the final result is shown in 24c.

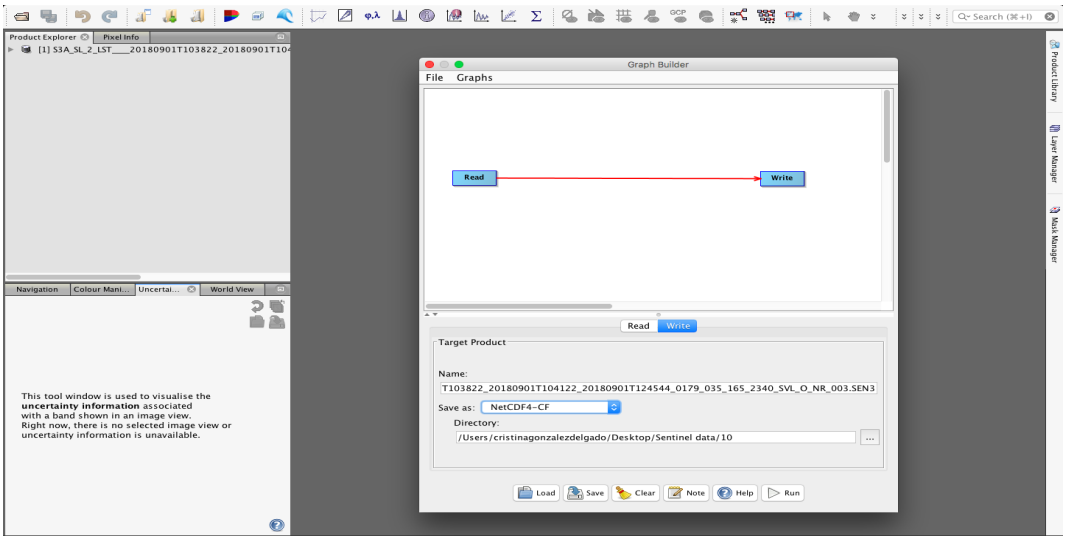

Figure 22: SNAP program. Each tile is written in NetCDF format

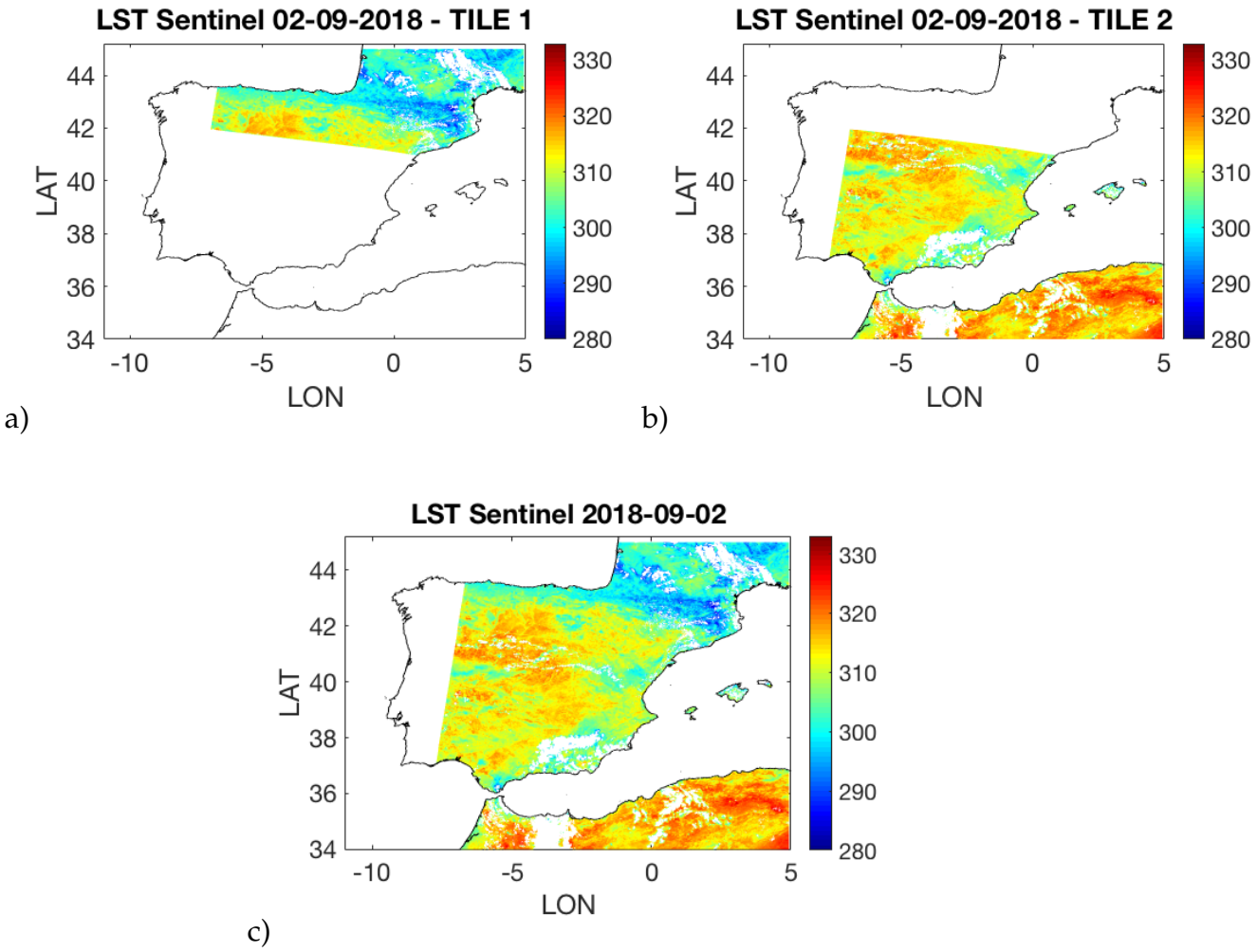

a) b) c)

Figure 23: a) and b) are the original LST tiles from Sentinel 3, whereas c) is the result obtained from merging them.

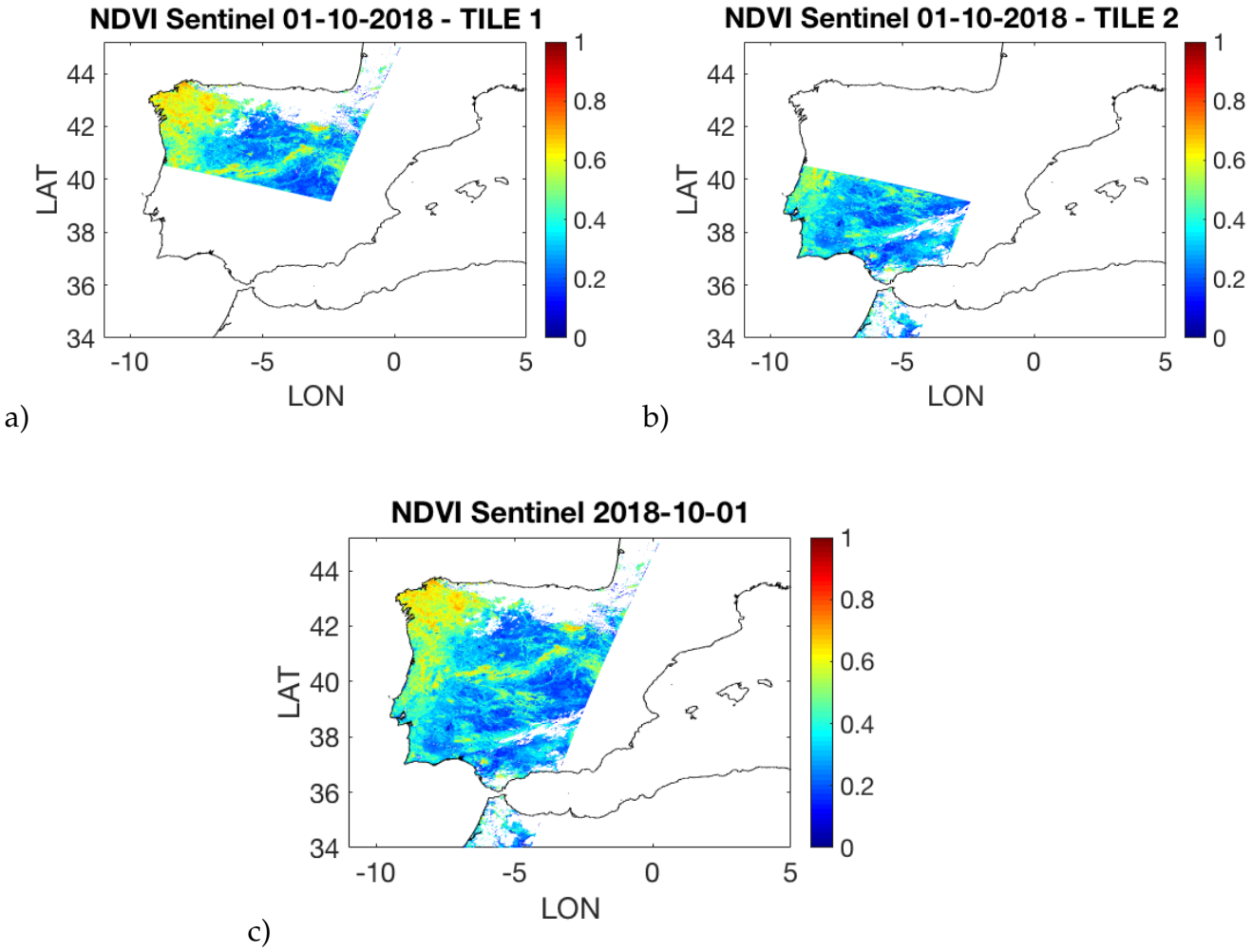

Figure 24: a) and b) are the original NDVI tiles from Sentinel 3, whereas c) is the result obtained from merging them.

Sentinel 3 LST Non-Time-Critical (NTC) products

Data characteristics and availability

NTC products are disseminated reporting the data of the whole orbit. Each NTC product consists of all the NRT products composing the orbit merged into one file. It means the orbit not only contains the tiles intersecting the area of interest but all the tiles worldwide generated during the orbit time period. NTC products have been subjected to extra processing steps to improve data quality.

These products are available in the long-term, they are not erased from the dataset.

Each file containing the whole orbit has an approximate size of 2 GB, and consequenty, you need a more powerful computer to process these files. They are less friendly to use than the NRT ones. It is in a native format .sen3.

NTC files download

The data is accessible via the Pre-Operations Data Hub. The steps to download the data are the same than the ones described for Near Real Time products, with the difference that "Non Time Critical" should be selected in timeliness filtering option. Figure 25 shows an example: the orbits covering the Iberian Peninsula.

After the filtering process, the orbits intersecting the chosen geographical area are displayed ready to be download (see figure 26).

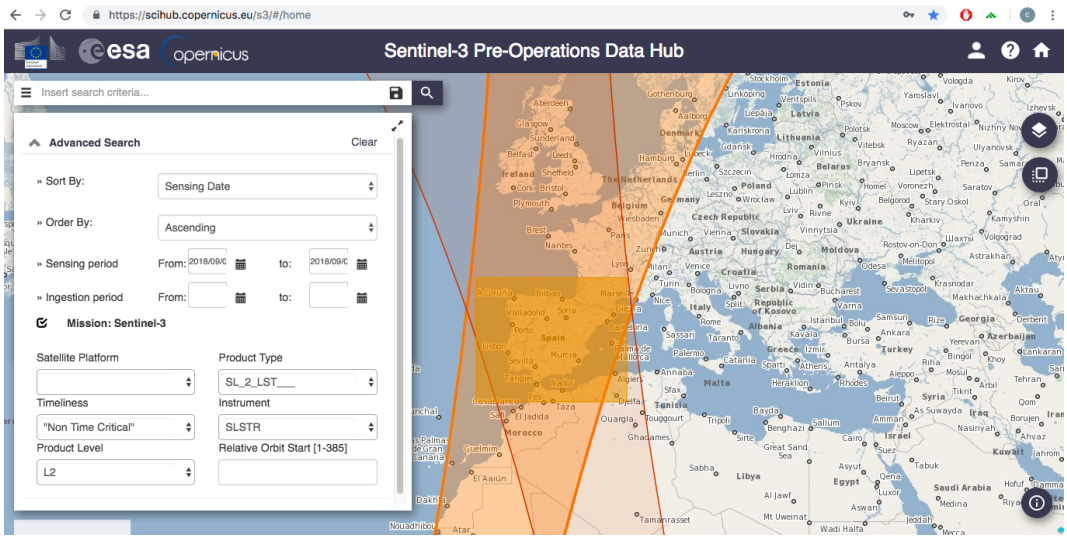

Figure 25: Sentinel 3 LST orbits covering the Iberian Peninsula. NTC files before applying the filtering process.

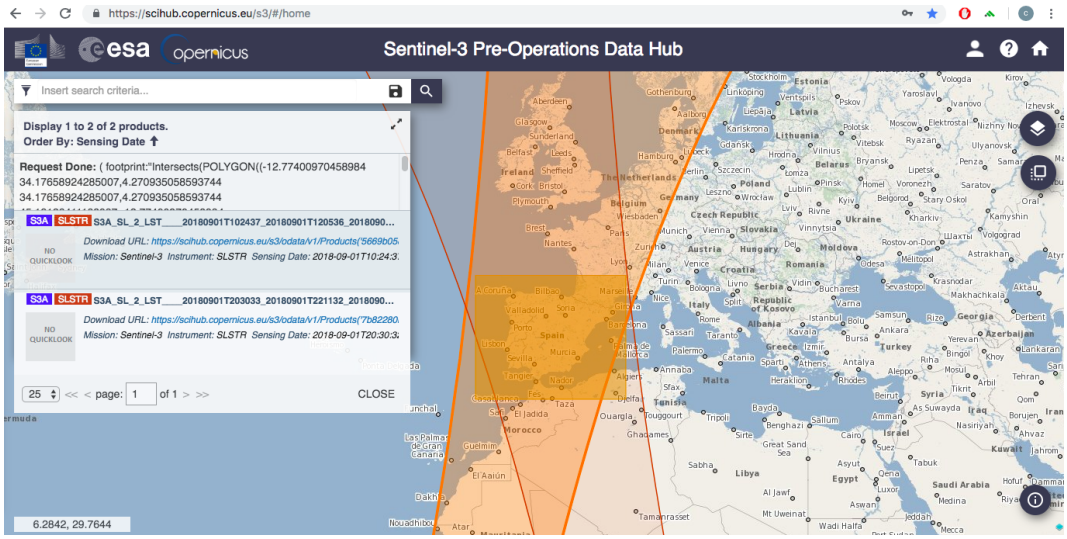

Figure 26: Sentinel 3 LST orbits covering the Iberian Peninsula. NTC files after applying the filtering process.

Preparation of the Sentinel 3 LST and NDVI data from NTC product
As well as for NRT products, it is necessary to rewrite the NTC Sentinel 3 LST data data into NETCDF format using the SNAP tool.

Given the big size of the file containing the orbit, the process inside SNAP to change to the new format is more demanding in terms of system resources. It is recommended at least 32 GB of RAM and a dedicated graphic card to run the appropriate functions without blocking the host resources.

In this project we have used NRT product for two reasons: it has been used a personal computer and also because the NTC platform was still in preparation.

4

DOWNSCALING ALGORITHM

In this chapter the downscaling algorithm developed at the UPC for distributing at BEC (Barcelona Expert Center) soil moisture maps at high resoltion (1 km) is described.

This algorithm is based on the synergy among three different products: SMOS L3 soil moisture at low resolution, and LST and NDVI at high resolution.
More detailed information about this algorithm can be found at Gerard Portal thesis [24]. This algorithm is an updated version of the original developed at the Maria Piles thesis [32]. The main differences is the use of an adaptive moving window.

4.1 DOWNSCALING ALGORITHM OVERVIEW

The aim of the downscaling algorithm developed at BEC by Gerard Portal, is to generate a high resolution Soil Moisture map from the original SMOS Soil Moisture measurement at low resolution ($TB \sim$ 30-40km): synergies with ancillary data (LST and NDVI) at high resolution is used.

The algorithm input data includes the low resolution Soil Moisture (L3 SM_{LR}), the Brightness Temperature (TB) at H and V polarizations, the Normalized Difference Vegetation Index (NDVI) and the Land Surface Temperature (LST).

The workflow of the downscaling algorithm, presented at figure 27, when using ancillary data from MODIS, includes the following steps:

1. Enhancement of L3 SM_{LR} map.
   It is possible that some of the SM_{LR} L3 maps on the pixels have no data. The low resolution L3 enhancement consists on estimating the value of these pixels.

by using L3 values from other nearby pixels and TB at 25 km at both H and V polarization over these pixels.

It is necessary to apply a two-step algorithm: First, the a_1, a_2 and a_3 coefficients are obtained using equation 21 at low resolution and over some surrounding pixels. Second, L3 SM values in the pixels originally without data, are calculated using the "a_i" values obtained at first step.

$$L3_{LR_{enhanced}} = a_1 + \frac{a_2}{3} * \sum_{i=1}^{3} TBv\theta_i + \frac{a_3}{3} * \sum_{i=1}^{3} TBh\theta_i \tag{21}$$

2. Aggregation of LST and NDVI to 25km.
   At this point, both the TB and the enhanced L3 are at low resolution (grid of 25 km), while NDVI and LST are at high resolution (1 km). It is necessary to aggregate both LST and NDVI to 25km so that they can be used in the linear equation described in next step.

3. Calculation of the linear equation coeficients b_i
   The linear equation 22 is applied first at low resolution to obtain the b_i coefficients. The TB, LST and NDVI at 25 km are substituted in the equation and the enhanced L3 SM, also at 25 km, is used as a reference to solve it.
   The first version of the algorithm obtained a set of "c_i" coefficients for all the study area. In this new version, the algorithm is applied several times on a much smaller area inside a moving window, that goes over all the area.
   The adaptive moving window allows to obtain a set of coefficients for each pixel rather than obtaining a unique set of coefficients for the whole area.
   Two windows are defined in order to maintain the pixel size of the window constant: a squared one of 5x5 pixels and another shape adaptive using 9 nearest neighbours points to the pixel of interest. The set of coefficients corresponding to each low resolution pixel is already calculated. Then, a map for each of the five coefficients is saved. These maps are interpolated from 25km to 1km.

$$SM_{LR_{enhanced}} = b_0 + b_1 LST + b_2 NDVI + b_3 TBh + b_4 TBv \tag{22}$$

4. Interpolation of TB from 25 km to 1 km grid
   In order to apply the linear equation at high resolution, it is necessary to grid all data to 1 km.
   NDVI and LST value were at 1km from the beginning, while TB and L3, that were

at 25 km, need to be interpolated 1km in order to have all the variables at 1km resolution.

5. Obtention of HR SM by applying the linear equation at high resolution
   Finally, once all data, including the coefficients maps are at HR, it is time to apply the linear equation at high resolution and obtain the HR SM, the one of the ancillary data (LST and NDVI).

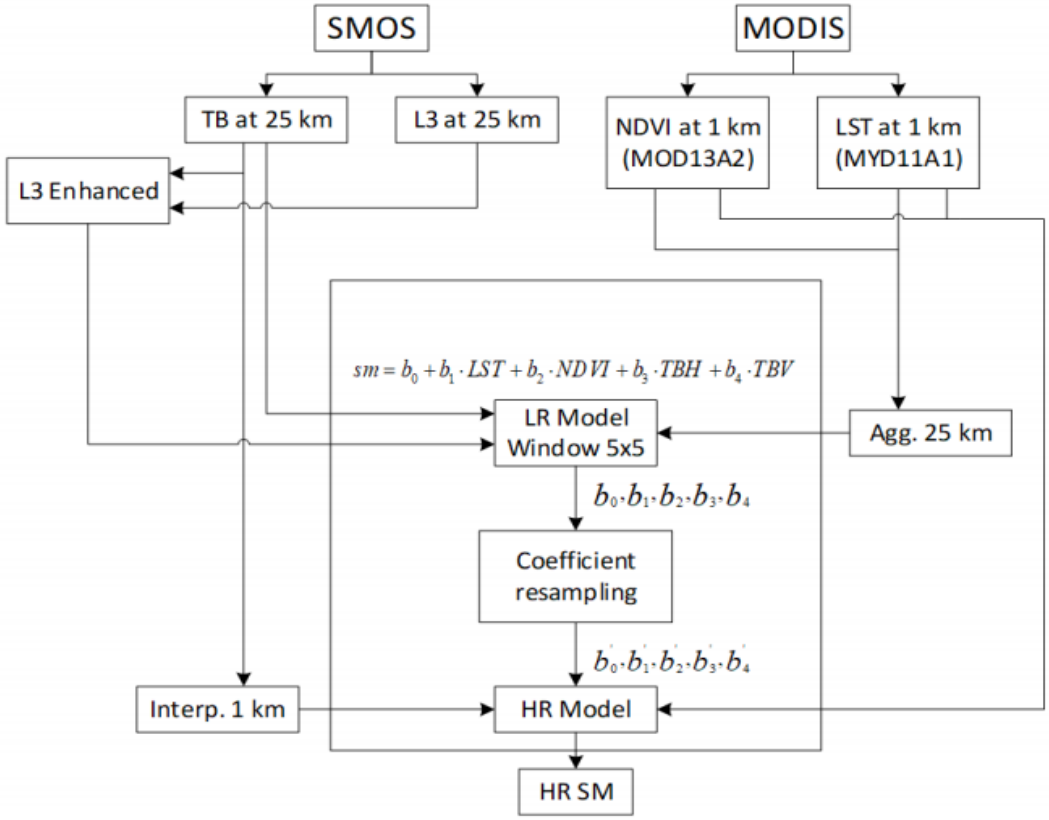

Figure 27: Downscaling algorithm flowchart, when using ancillary data from MODIS (NDVI and LST at 1km resolution), and SM_{LR} L3 and TB from SMOS.

In the next section a description of the different variables used in the algorithm is presented.

4.2 LOW RESOLUTION SOIL MOISTURE (SM_{LR})

The SM_{LR} is obtained from SMOS, specifically it is provided by the Barcelona Expert Center (BEC).

The SMOS revisit time is every 3 days, which means that global coverage is achieved combining images from 3 days. Each 9 days the orbit crosses the same exact point. This is the reason why BEC provides daily, 3-days, 9-days, monthly and annual products.

We will use as input for the downscaling algorithm the daily SM_{LR} L3 product. The maps are separated in ascending or descending orbit. It is obtained from level-2 product by interpolating to a 25km grid. Before the interpolation, a quality-filtering process is performed and negative humidity values are eliminated. Also, every value receives a quality index, which indicates in which measure this pixel is affected by the Radiofrequency Interference (RFI).

4.3 BRIGHTNESS TEMPERATURE (TB)

TB L1C information is also provided by SMOS, by the Barcelona Expert Center (BEC). There are two variables inside TB L1C, corresponding to the vertical (TB_v) and horizontal (TB_h) polarizations. These measurements are taken from three different incidence angles (32.5, 42.5 and 52.5) and two orbits per day (descending and ascending).

The mean TBΘ_p is calculated in the following way:

$$C = \frac{TB\Theta_p 32.5 + TB\Theta_p 42.5 + TB\Theta_p 52.5}{N} \tag{23}$$

where p is the polarization (vertical or horizontal) and N is the total number of measurements. If none of the measurements is valid, meaning that N is 0, TB_p will be considered invalid.

4.4 LAND SURFACE TEMPERATURE (LST)

The first version of the downscaling algorithm has used as ancillary data the LST and the NDVI at 1km from MODIS (Aqua NASA mission). In this project the objective is to analyze the LST provided by Sentinel 3 recently launched. A detailed comparison at LST level and at the SM_{LR} L3 high resolution is done. In order to see if Sentinel 3 product could substitute the MODIS one.

LST from MODIS
The LST information retrieved from MODIS on board of Terra and Aqua missions, can be obtained by two different algorithms: the split-window algorithm and the day/ night algorithm. The split window algorithm, which is the one used as input

for our algorithm, retrieves the data daily at 1km grid.
We will use only LST provided by Aqua (MYD11A1), which provides data closer to the maximum temperature hours of the day and it was the data used in the first version of the downscaling algorithm with adaptive sliding window.
Miriam Pablos PHD demonstrated that best results are obtained when using the maximum temperature of the day instead of using the LST colocated to SMOS measurements.
The LST values below 2 K are eliminated before using them in the algorithm.

LST from Sentinel 3
The LST information is acquired by Sentinel 3 daily, in a 1km grid. There are available two different products: The Near Real Time product (NRT) and the Non Time Critical (NTC) products.
The NRT product contains the individual tiles, uploaded hours after their acquisition. The (NTC) product contains the data of the whole orbit with a higher quality processing level.
We use the NRT product as input data of the algorithm due to two reasons: One of them has been the computational resources. The NRT products have a size of 60MB approximately, while the NTC products of 2.5 GB. The second one is that if we want to obtain the NRT downscaling maps it is necessary to use data uploaded close to the acquisition moment.

4.5 NORMALIZED DIFFERENCE VEGETATION INDEX (NDVI)

This project has also the aim of comparing NDVI from MODIS and Sentinel 3, and their use as ancillary data in the downscaling algorithm for obtaining high resolution SM maps.

NDVI from MODIS
NDVI information is obtained by MODIS instrument on board of Terra and Aqua missions. Specifically, we have used only Terra product (MOD13A2), which is the one used originally to develop the downscaling algorithm [32].
The NDVI is produced with a temporal resolution of 16 days and at 1km grid spatial resolution. NDVI is considered much more stable than LST. Consequently, it is not necessary to use a daily product. This 16-day product has the advantage of being free cloud-efect.

NDVI from Sentinel 3
NDVI from Sentinel 3 is obtained daily with 1 km spatial resolution. It is included inside the same packet containing the LST as ancillary data.

5

RESULTS

The downscaling algorithm to compute HR SM maps, developed at UPC [24] and applied at BEC for distributing soil moisture maps at high resolution, has been described. This algorithm requires as input data the TB, L3 (LR SM), NDVI and LST.

The aim of this section is to describe the LST and NDVI products provided by MODIS and Sentinel 3, and compare experimentally the differences in the computed HR SM maps.

5.1 LAND SURFACE TEMPERATURE (LST) COMPARISON

This section describes the experiments and results of the comparison between the LST data from MODIS and Sentinel 3, and the differences in the obtained HR SM maps when using one or the other LST data.

As input data for the algorithm, we use the TB, L3 and NDVI from MODIS, and the LST from both MODIS and Sentinel 3.

The months used for the comparison are September and October 2018. There are two main reasons why no more months have been included: Firstly, as mentioned in section 3.5.1, we are using NRT data from Sentinel 3, since NTC required higher computational resources. NRT data is erased from the repository after one month and it is not longer accessible, which means that there is not the possibility of downloading past data. Secondly, the manual and time-consuming data download and pre-processing process.

The evaluation is performed by means of three different experiments:

- Experiment 1: Computation of HR SM maps averaging every 4 days, using data of September and October 2018.

- Experiment 2: Computation of HR SM maps averaging 15 days, using data of September and October 2018.

- Experiment 3: Computation of monthly average HR SM maps of October 2018.

Each experiment will include also a direct comparison of the average LST from MODIS and Sentinel for the interval of interest. In order to understand the variation between the two HR SM maps, it is necessary to analyze first the LST from MODIS and Sentinel differences.

The specific process to obtain the HR SM maps for each experiment includes two steps: The first step consists on averaging the daily maps (of TB, L3, NDVI and LST) corresponding to the period of interest. The second step is actually run the HR SM map algorithm using as input the averages of each type of data. This second step will be repeated twice, using the LST from MODIS and then the LST from Sentinel 3.

5.1.1 *Experiment 1: 4 days average high resolution soil moisture map (HR SM map)*

In this first experiment, we will compare the high resolution soil moisture HR SM maps obtained using the LST from MODIS and Sentinel 3 averaging every 4 days, which is the time it takes Sentinel to complete a cycle over the whole Iberian peninsula (see figure 28).

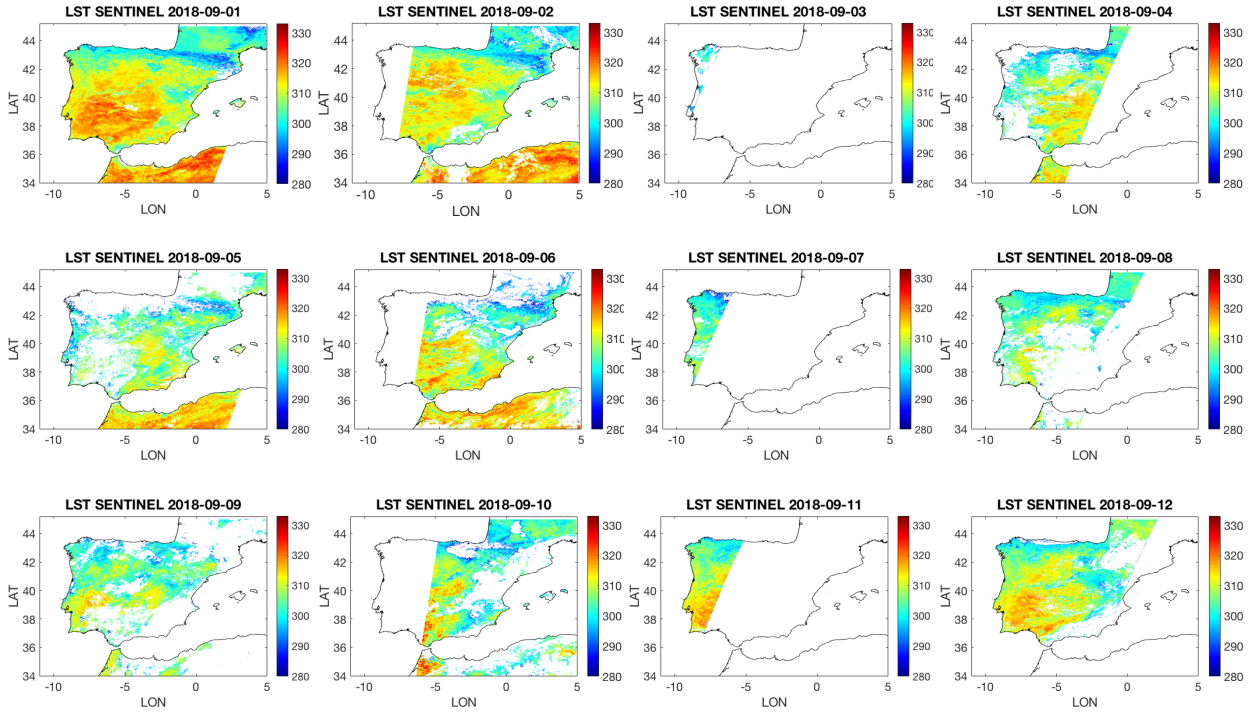

Figure 28: Sentinel 3 LST maps cycle. Daily LST provided by Sentinel 3 from 1st to 12th of September 2018.

Find the comparison of 4 days average LST maps from MODIS and Sentinel 3 in figure 29, that may help later to infer the cause of the variation of HR SM maps.
The mean error μ range in the studied period is between 0.11619 and 1.2 K, while the standard deviation θ is $\sim$ 2 K.
In the case of October 2018, we can see in the histogram that the peak is slightly moved to the right. This is because the acquisition time of MODIS and Sentinel 3. MODIS obtains the temperatures from 12:30-13:30h, while Sentinel 3 from 9:30-11h, when the temperatures are lower. It seems that in October the changes of the temperature during the time gap between acquisitions time changed more than in September.

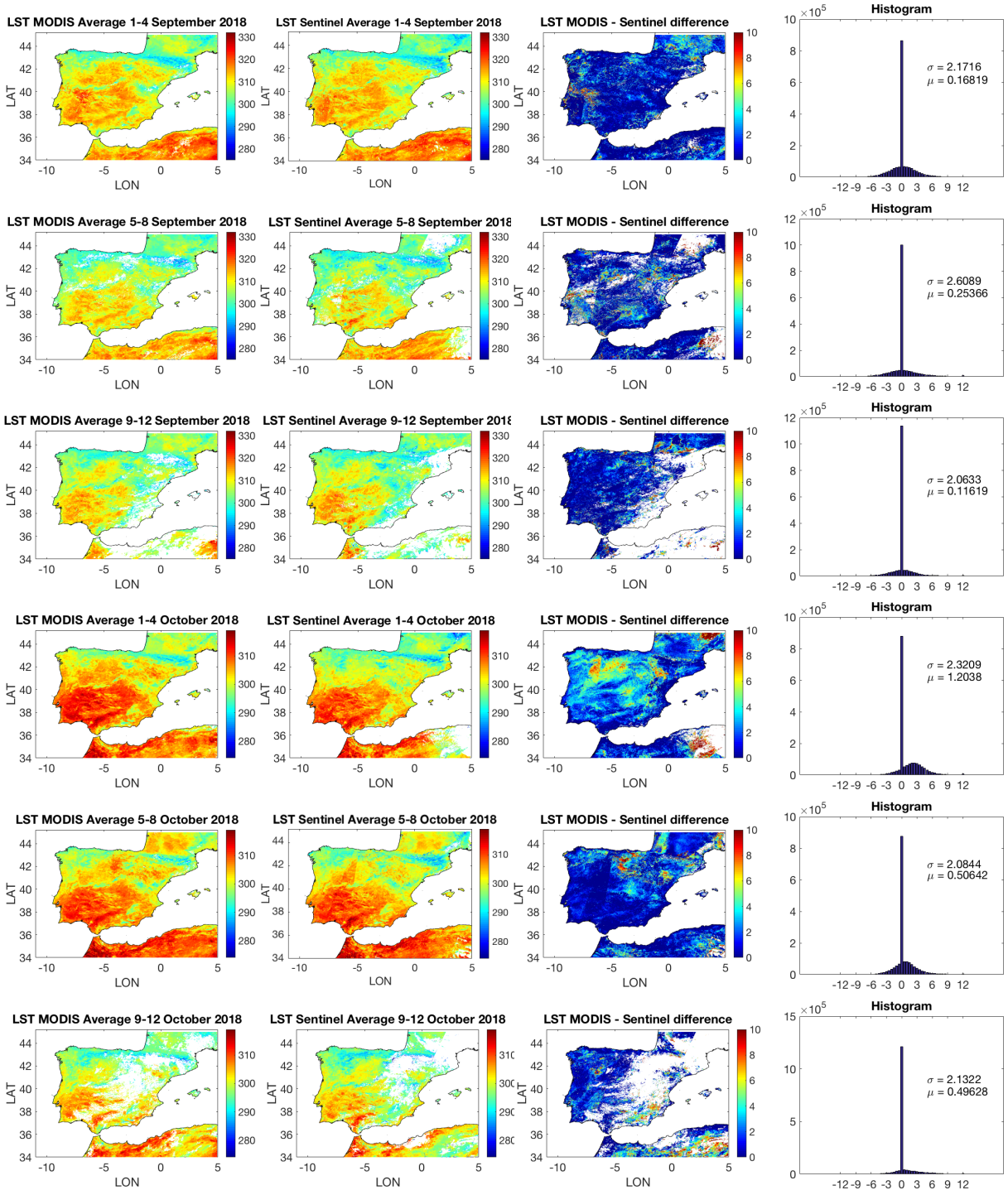

Figure 29: September and October 2018 4-days average LST from MODIS and Sentinel 3. The first column presents the mean MODIS LST every 4 days, the second column shows the mean Sentinel 3 LST every 4 days, the third column is the difference between MODIS and Sentinel 3 LST 4-days average and the fourth column is the histogram from the third one.

Figure 30 shows the HR SM maps computed using 4-days average LST.
The mean error range μ is $0.00014099 - 0.0003741$, while the standard deviation θ is around 0.02.
We can see that the HR SM differences are distributed more or less homogeneously and the zones more affected by variations do not correspond clearly to the zones where the LST is different.

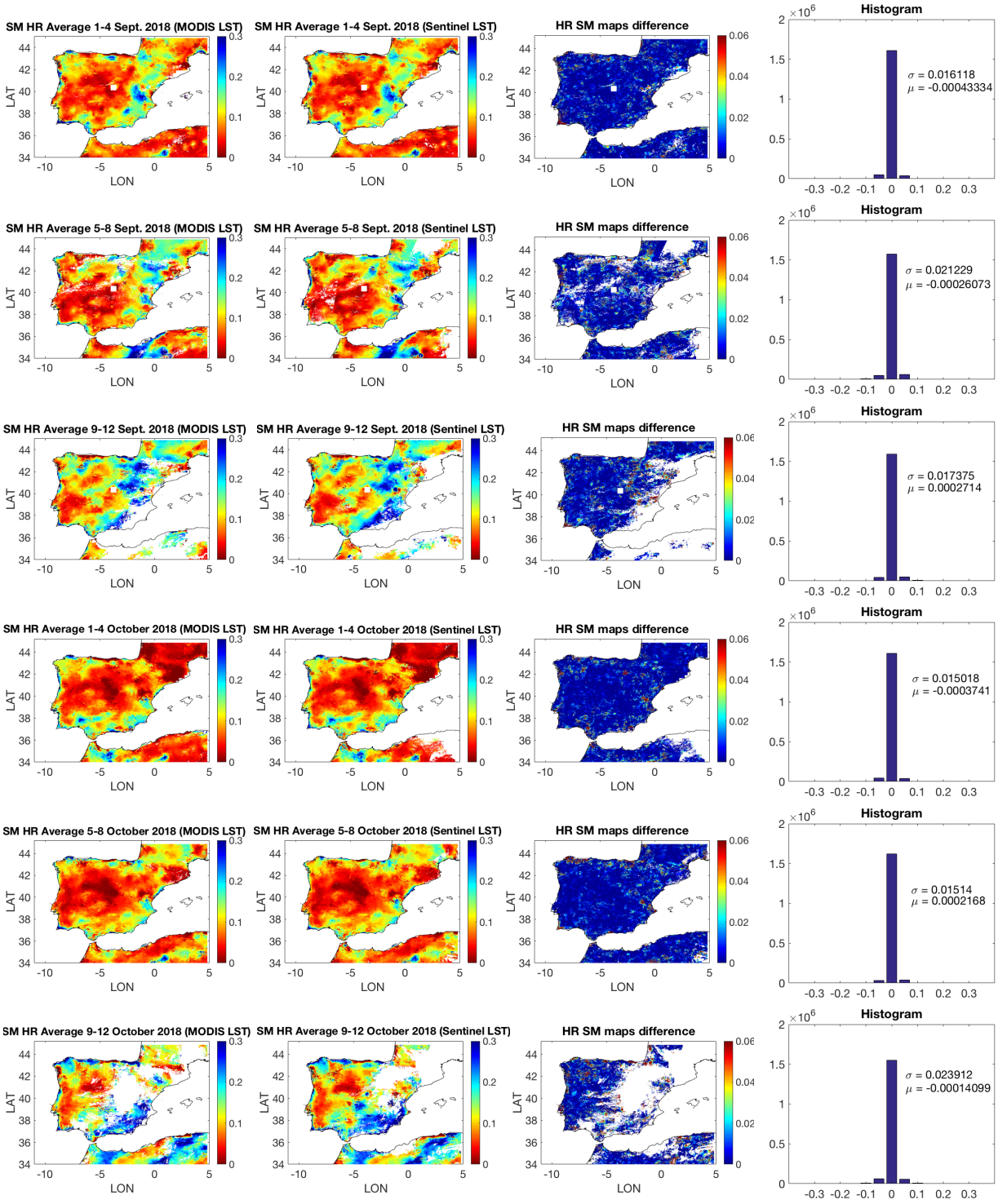

Figure 30: September and October 2018 4-days average HR SM maps using LST from MODIS and Sentinel 3. The first column is the HR SM obtained by using MODIS 4-days average LST, second column is the HR SM obtained using Sentinel 3 4-days average LST, the third column includes the difference between HR SM computed using LST from MODIS and Sentinel 3 and the fourth column is the histogram of the third one.

5.1.2 *Experiment 2: 15 days average high resolution soil moisture map (HR SM map)*

This second experiment compares the HR SM obtained from a 15 days average using LST from MODIS and Sentinel 3.
Specifically, we studied three different 15 day periods: the 15 first days of September 2018 and the 15 first and last days of October 2018.

SM HR from first 15 days of September 2018
Find below (figure 31) the LST images from MODIS and Sentinel 3 corresponding the September 2018 15 first days interval, including the map of differences and its histogram.
The differences map shows where the variation is more relevant, in this case, the coast side in the Murcia region and east Andalucia areas and a part of south Catalonia and Central Aragon.
Regarding the histogram, we can see that the mean and standard deviation are $\mu = 0.2684$ and $\theta = 1.8978$ K.
One of the observations that can be done from a) and b) is that in general, LST values in MODIS are higher than in Sentinel 3. It has sense since MODIS acquires data from 12:30 till 13:30h, while Sentinel gets it from 9:30h till 11:00h (depending on the day).

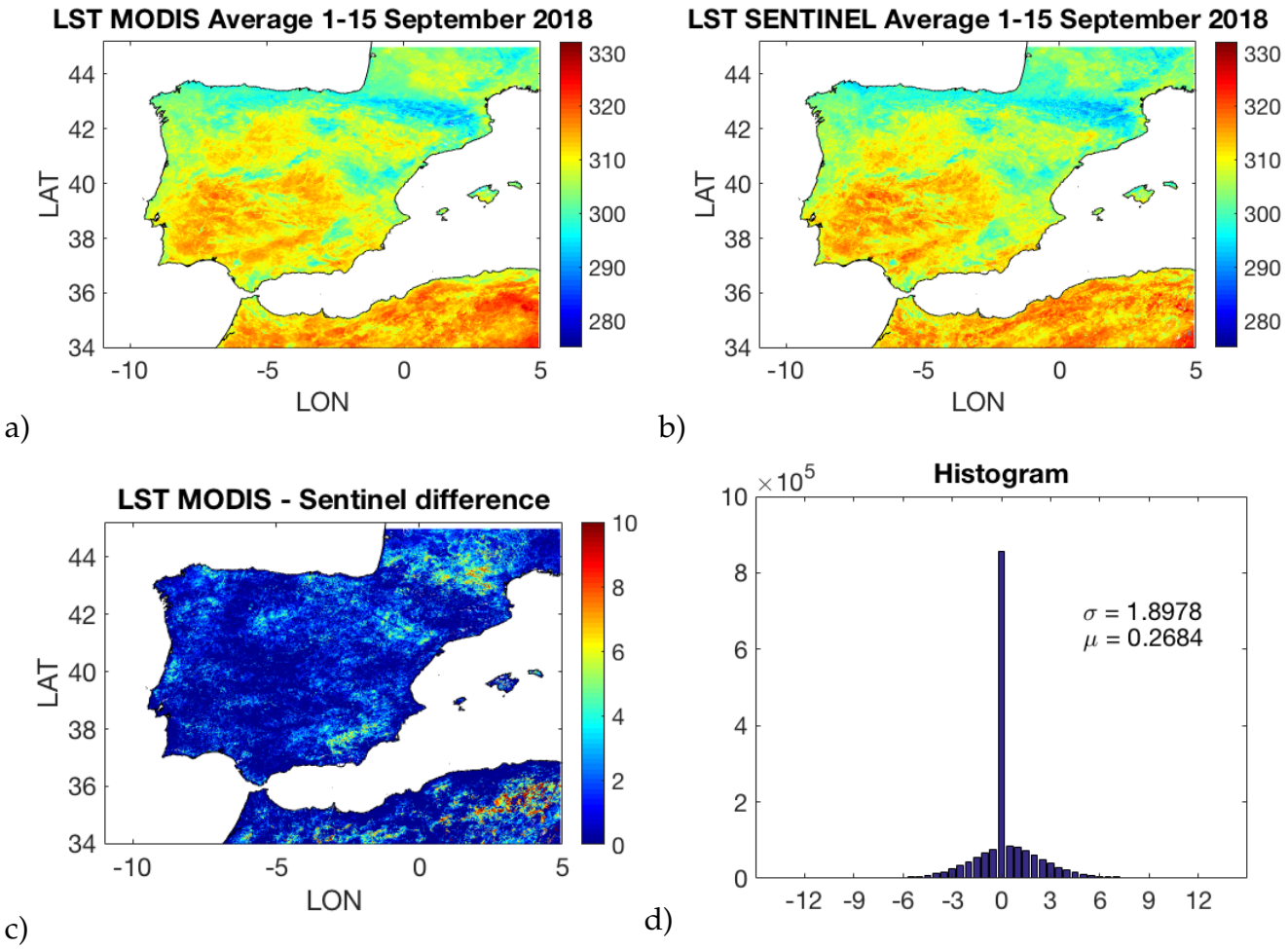

Figure 31: a) and b) are the 15-days averagde LST from MODIS and Sentinel 3 respectively, c) presents the result of the substraction: Modis LST - Sentinel-LST, and d) is the histogram obtained from c)

Find below the HR SM maps of September 15 first days average using the LST from Sentinel 3 and MODIS respectively (figure 32).
It can be seen that the differences are randomly distributed in the Iberian Peninsula. The most affected zones do not correspond directly to the ones where LST varies.

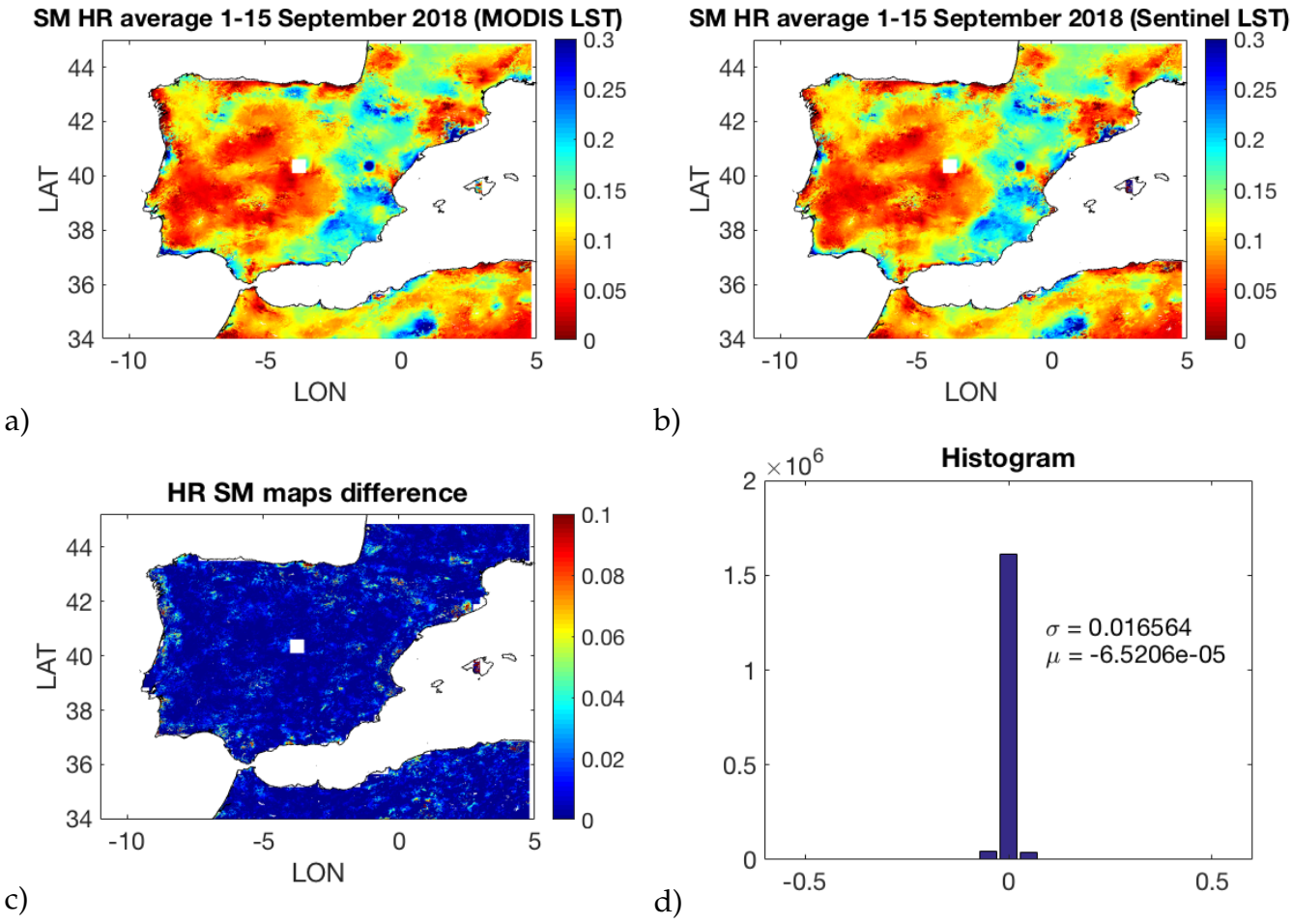

Figure 32: a) and b) are HR SM maps using LST from MODIS and Sentinel 3 respectively, c) is the result of the substraction: Modis HR SM - Sentinel 3 HR SM, and d) is the histogram obtained from c)

SM HR from 15 first days of October 2018

Let's focus in the 15 first days of October.

Find below the LST average obtained from Sentinel 3 and MODIS, their differences map and histogram in figure 33.

As mentioned before, we clearly observe in the differences map and its histogram that the LST from MODIS includes higher values. MODIS sensing time corresponds to the maximum temperature hours of the day, while Sentinel 3 acquires the data earlier in the morning, when the temperature has not reached its maximum yet.

In this case, we see that the temperature variation is distributed covering almost all Iberian Peninsula, being specially pronounced in four geographical points, corresponding to north-west,south-west and north-central regions of the Iberian Peninsula.

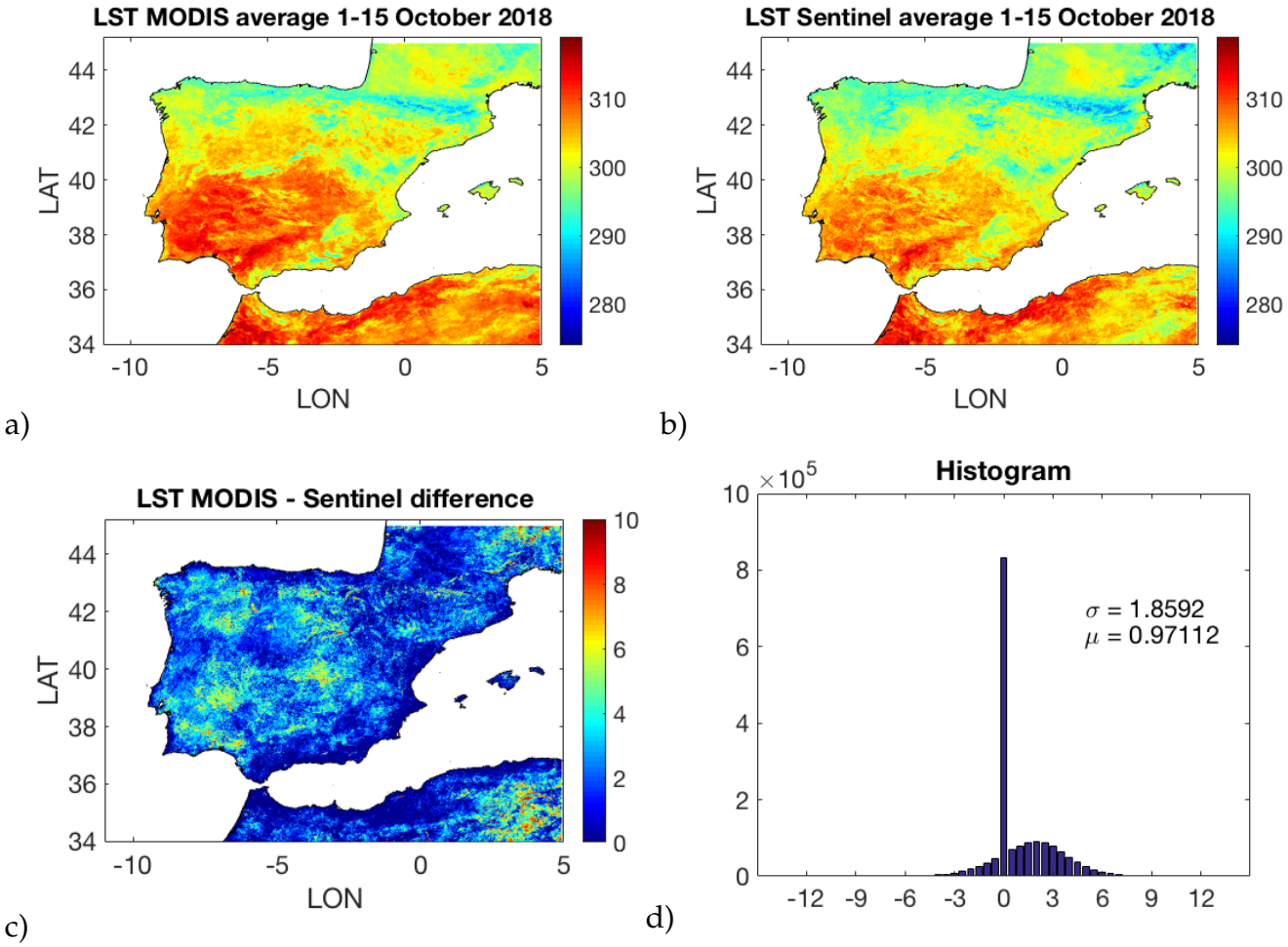

Figure 33: a) and b) are the LST maps from MODIS and Sentinel 3 respectively, c) is the result of the substraction: Modis LST - Sentinel 3 LST, and d) is the histogram obtained from c).

Figure 34 shows the HR SM moisture maps. Again the zones affected by differences do not correspond to the ones where LST dissimilarities are more marked. The histogram mean $\mu = -2.8291e^{-06}$ and standard deviation $\theta = 0.011974$ are very small, which indicates that the values of the HR SM maps are very similar and the degree of variation remains more or less uniform over the geography.

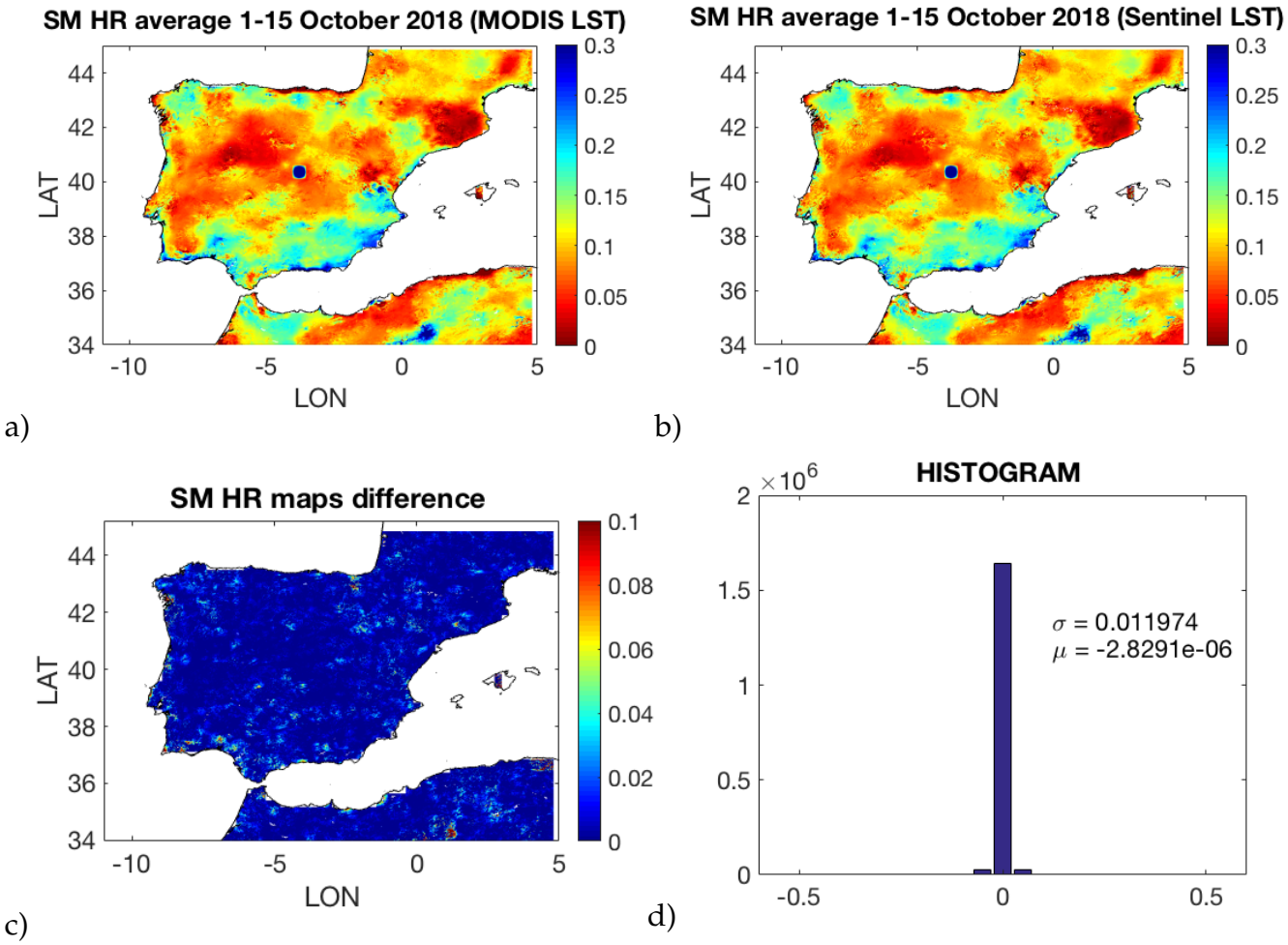

Figure 34: a) and b) are the HR SM maps using LST from MODIS and Sentinel 3 respectively, c) is the result of the substraction: Modis HR SM - Sentinel 3 HR SM, and d) is the histogram obtained from c)

SM HR from second 15 days of October 2018

Finally, let's focus in the second 15 days of October 2018.

Figure 35 includes the LST 15-days average maps from Sentinel 3 and MODIS, their differences map and the corresponding histogram.

In this time interval, the temperature variation is specially noticeable in a specific region of the geography, reaching its maximum approximately at the central part of the Iberian Peninsula geography.

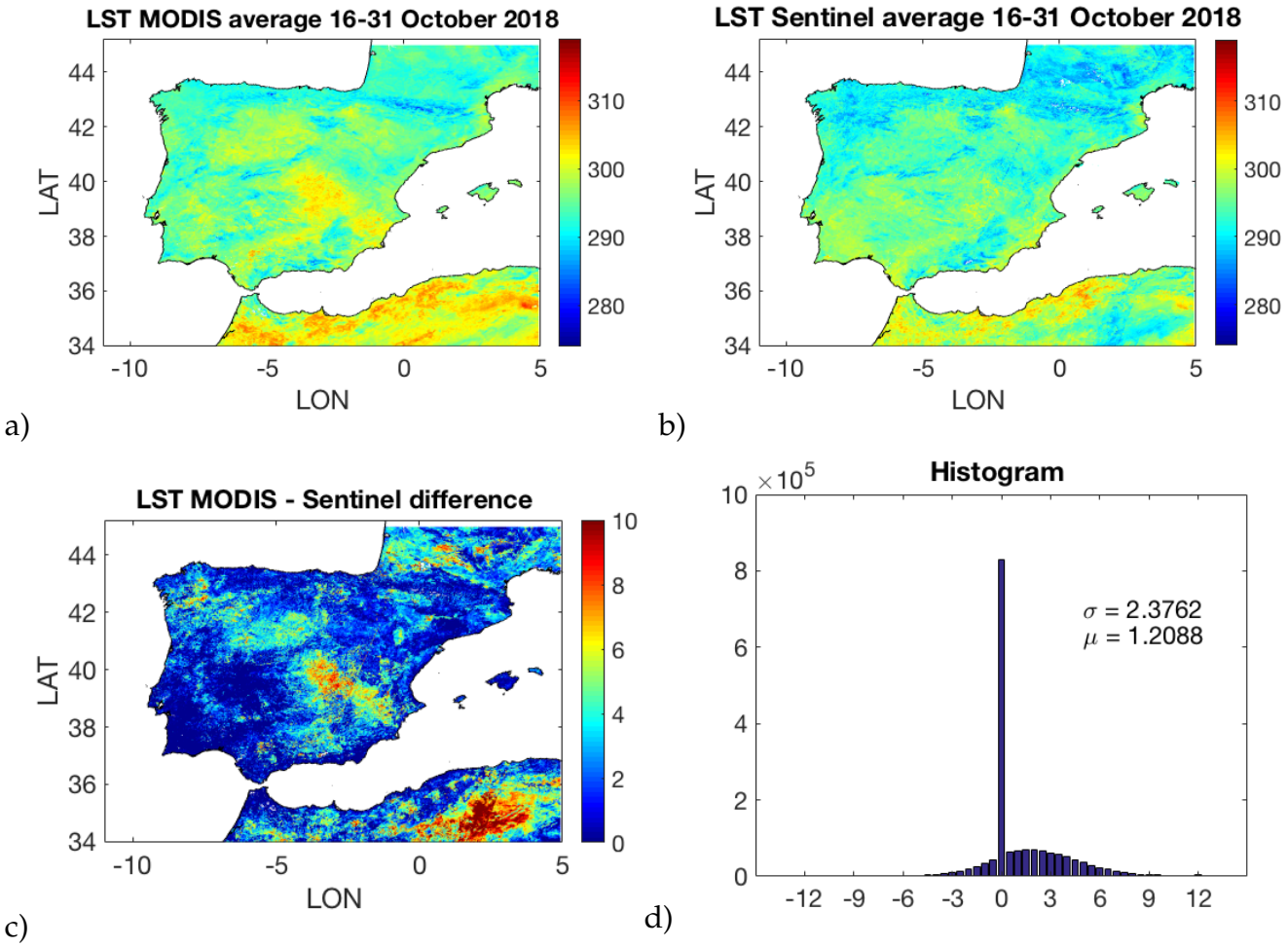

Figure 35: a) and b) are the LST from MODIS and Sentinel 3 respectively, c) is the result of the subtraction: Modis LST - Sentinel 3 LST, and d) is the histogram obtained from c).

The HR SM maps corresponding to this period are shown in figure 36. Even though there was a clear zone of difference in the LST maps, we cannot see that this region is more affected in the HR SM maps. There is not a clear or direct relationship between the variation in the LST and the HR SM maps.
Also, as in the first two cases, the mean error μ is of the order of $\sim 10^{-4} \sim 10^{-5}$.

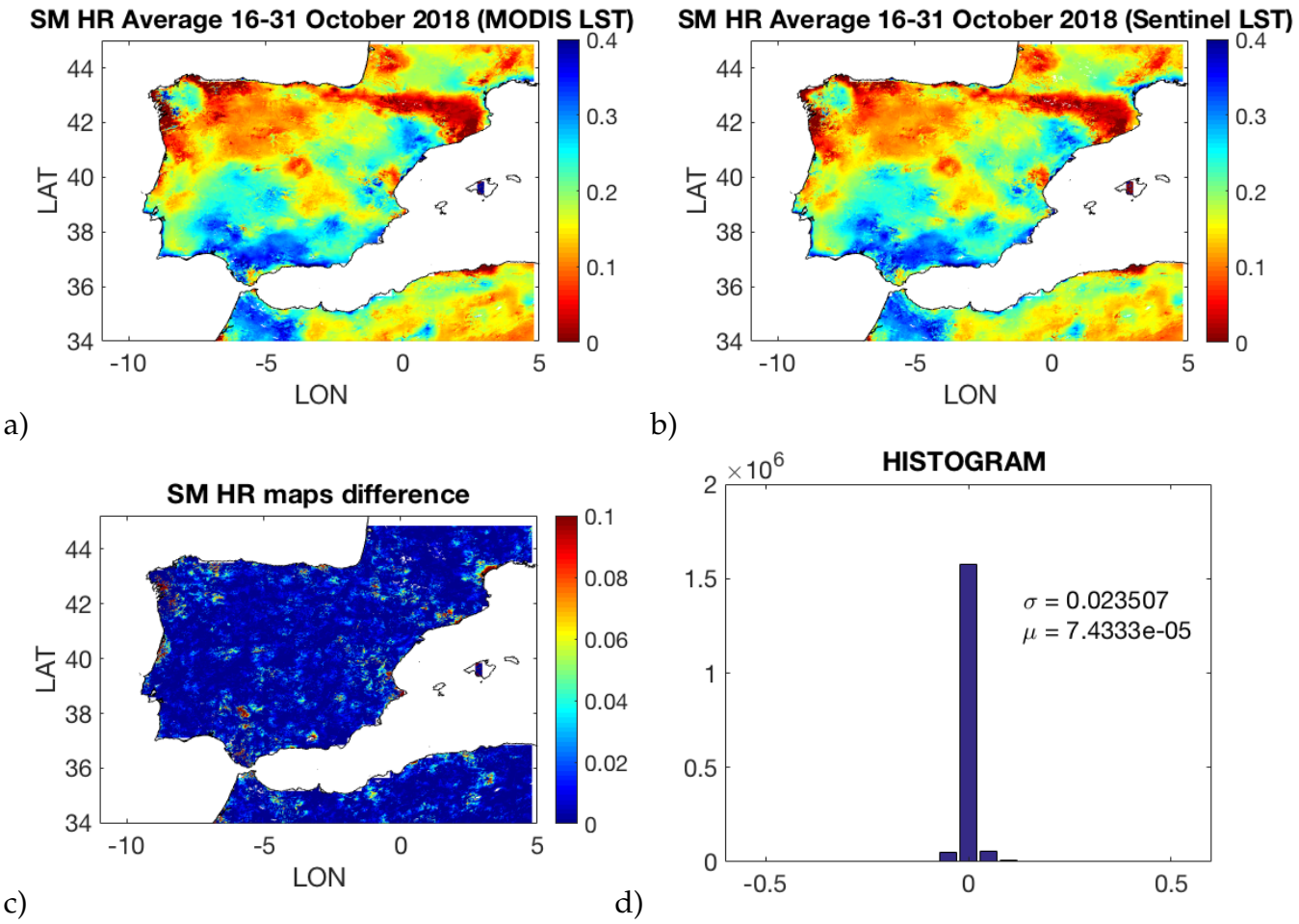

Figure 36: a) and b) are the HR SM maps using LST from MODIS and Sentinel 3 respectively, c) is the result of the subtraction: Modis HR SM - Sentinel 3 HR SM, and d) is the histogram obtained from c).

5.1.3 *Experiment 3: Monthly average high resolution soil moisture map (HR SM map)*

This third experiment aims to study the differences in LST and HR SM maps averaging 1 month data.
Find in figure 37 the LST monthly average of October 2018, computed from daily maps of MODIS and Sentinel 3 respectively.
As it can be seen, the difference is more or less uniform except in two specific points located approximately in the central and the south-west part of the Iberian Peninsula.

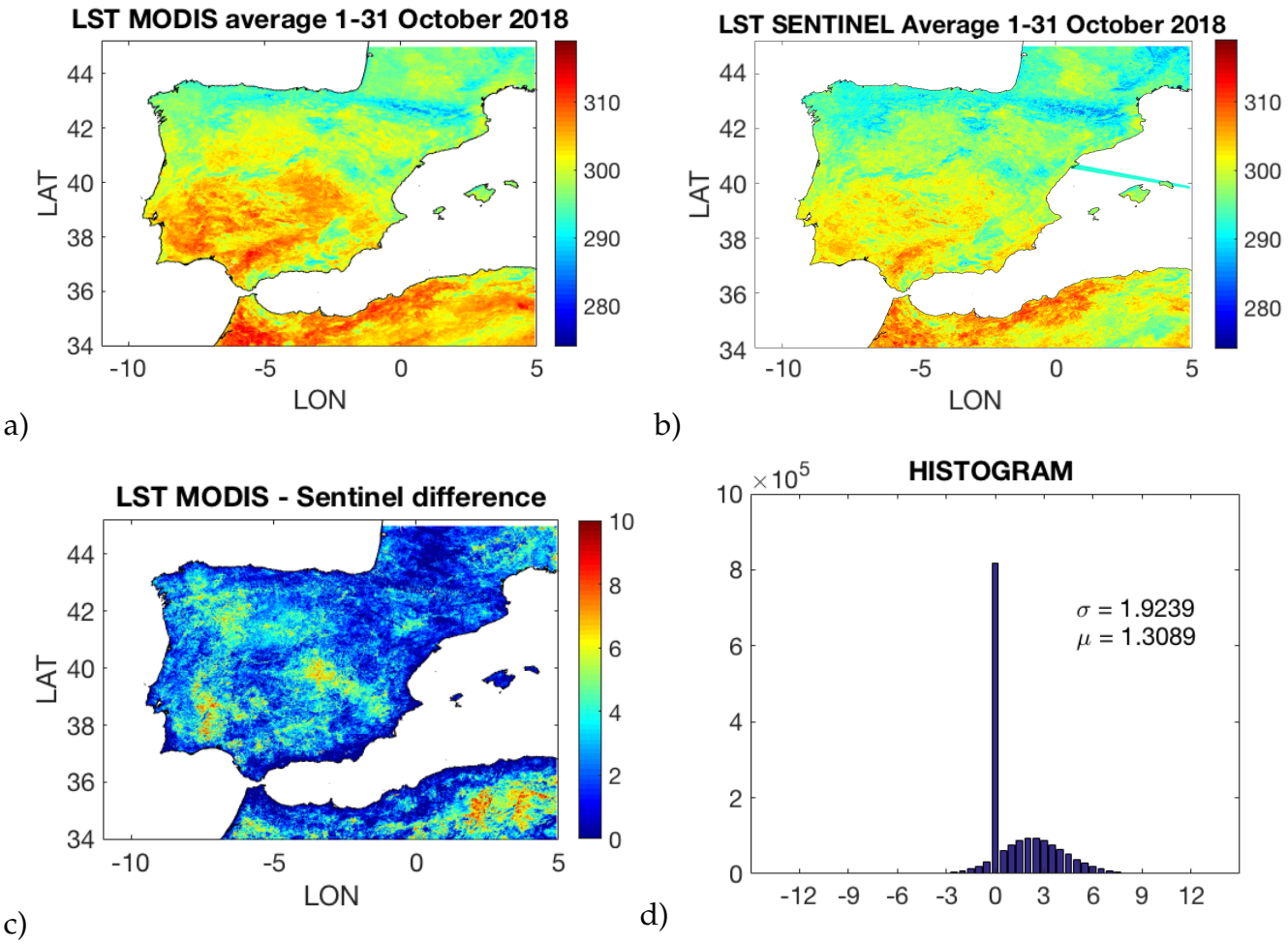

Figure 37: a) and b) are the LST from MODIS and Sentinel 3 respectively, c) is the result of the subtraction: Modis LST - Sentinel LST, and d) is the histogram obtained from c)

Regarding HR SM maps (Figure 38), we see again that they are very similar when using LST from MODIS and Sentinel 3. The mean error μ and the standard deviation θ of the differences map histogram are 0.00011315 and 0.013479 respectively, very similar to the mean error and standard deviation when averaging every 4 and 15 days, as seen in the two previous experiments.
Again, there is not a clear relationship between the areas more affected by LST variations and the ones in the HR SM maps computed from the LST.

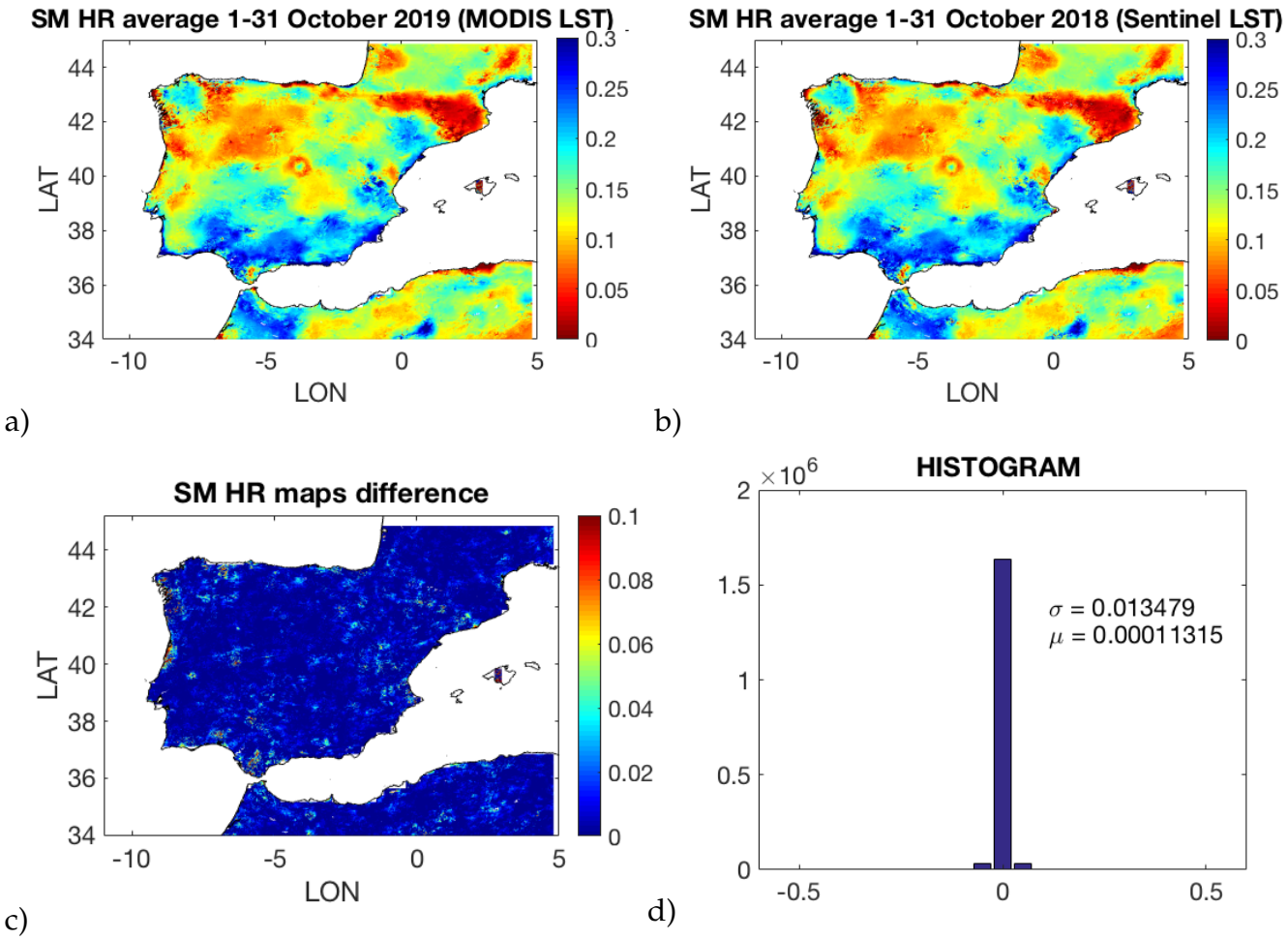

Figure 38: a) and b) are the HR SM maps using LST from MODIS and Sentinel 3 respectively, c) is the result of the subtraction: Modis HR SM -Sentinel 3 HR SM, and d) is the histogram obtained from c)

5.2 NORMALIZED DIFFERENCE VEGETATION INDEX (NDVI) COMPARISON

In this section we will compare the two different NDVI products from MODIS and Sentinel 3 and the resulting HR SM maps.

5.2.1 *NDVI products characteristics and preparation for the comparison*

The MODIS NDVI we will use is a 16-days product with a resolution of 1km.
Sentinel 3 NDVI is provided daily with a 1km resolution. As mentioned in previous sections, it is included inside the L2-LST product from SLSTR as an ancillary product.

Before the comparison itself, it is worth analyzing why MODIS provides NDVI 16-days products instead of daily ones. Figure 39 shows the daily NDVI evolution provided by Sentinel 3 for 16 days of October 2018 (there is not information of October 15th).
At first sight we can conclude that the day-to-day variation of the NDVI is not meaningful, which is probably the reason why MODIS provides a 16-day product instead of a daily one.

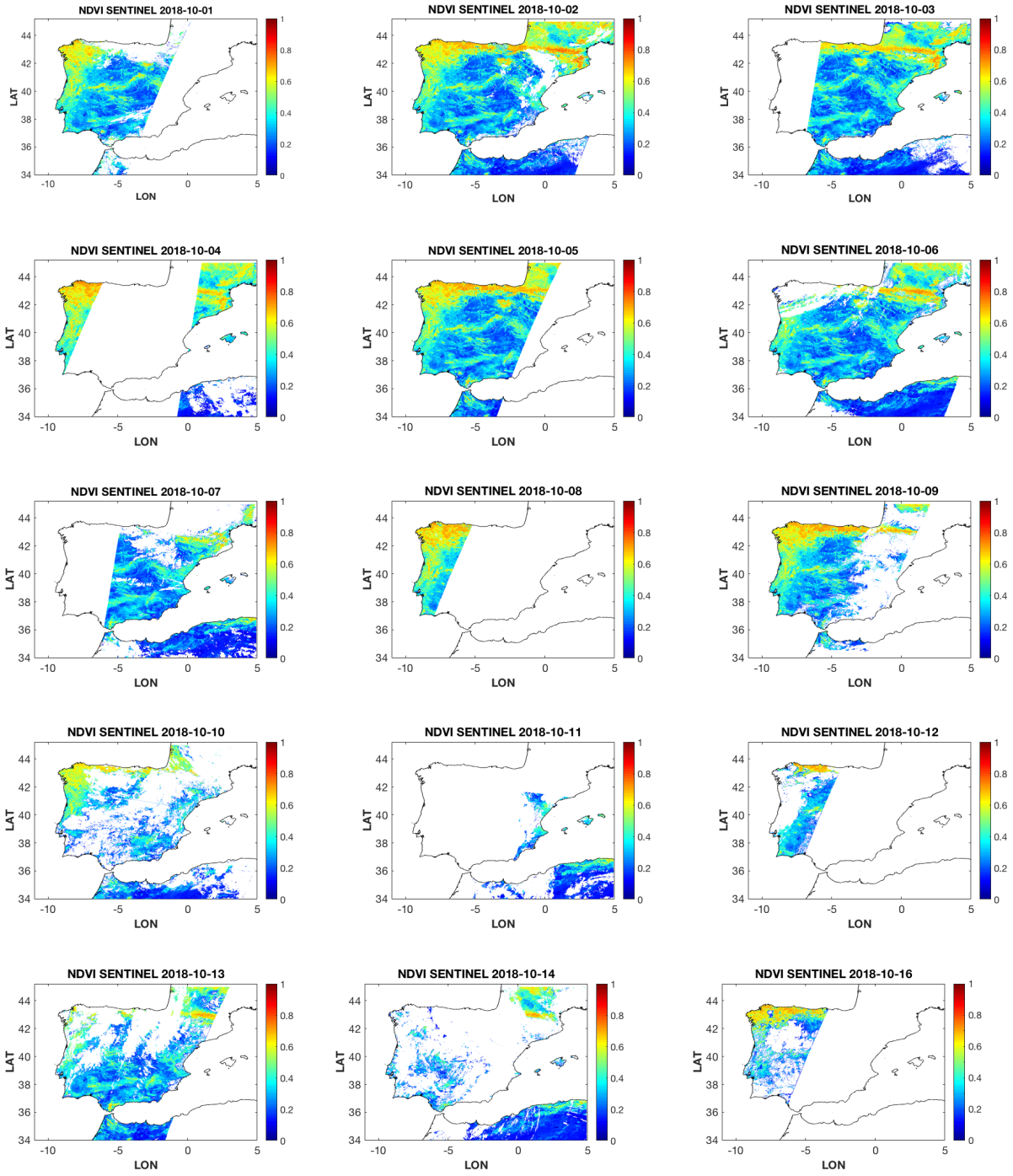

Figure 39: NDVI from Sentinel 3 daily evolution

In order to perform the comparison of the NDVI, it is necessary to build a 16-day product from daily NDVI information provided by Sentinel 3, following an algorithm

as close as possible to the one that MODIS uses to build its NDVI 16-day product.
The MODIS 16-days product is computed by choosing the best available pixel value from all the acquisitions of the 16 day period. The criteria used is low clouds, low view angle and the highest NDVI [6].
We compare two different algorithms to build the 16-days product in order to select the one that provides a product closer to the 16-days product from MODIS. The first algorithm averages the daily maps, ignoring the pixels without information, either because in a particular day there is not information of this geographical zone or because of the clouds effect. The second one selects the pixels with higher value instead.

Figure 40 shows the 16-days NDVI product for MODIS, the 16-day product built by averaging daily Sentinel 3 maps and then the one by choosing the highest value. We can conclude that the second approach leads to a more similar NDVI 16-days map. So, it will be used for the comparison.

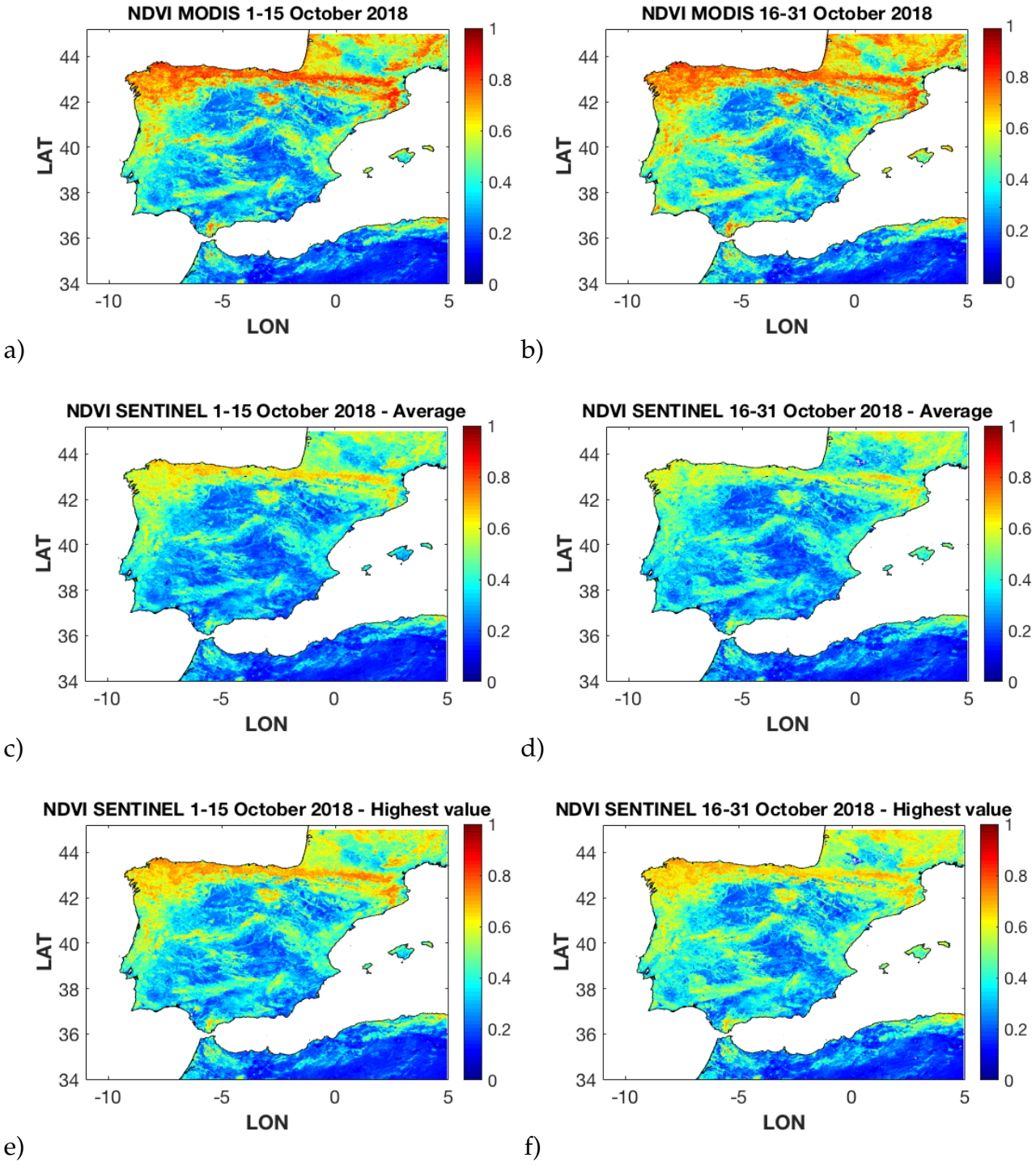

Figure 40: 16-days NDVI from MODIS and Sentinel 3. a) and b) show the NDVI from MODIS, c) and d) show the NDVI from Sentinel 3 calculated as an average of pixel values, and e) and f) show the NDVI from Sentinel 3 obtained by keeping the most reliable and higher pixel values.

5.2.2 *Comparison of 16-days NDVI and resulting HR SM maps*

As stated in previous section, we will compare the 16-day NDVI product from MODIS and the 16-day product built from choosing the highest pixel value from daily NDVI maps provided by Sentinel 3.

Figure 41 shows the HR SM maps obtained by using 16-days product from MODIS and the 16-day average computed from daily NDVI Sentinel 3 data (choosing the highest pixel value).

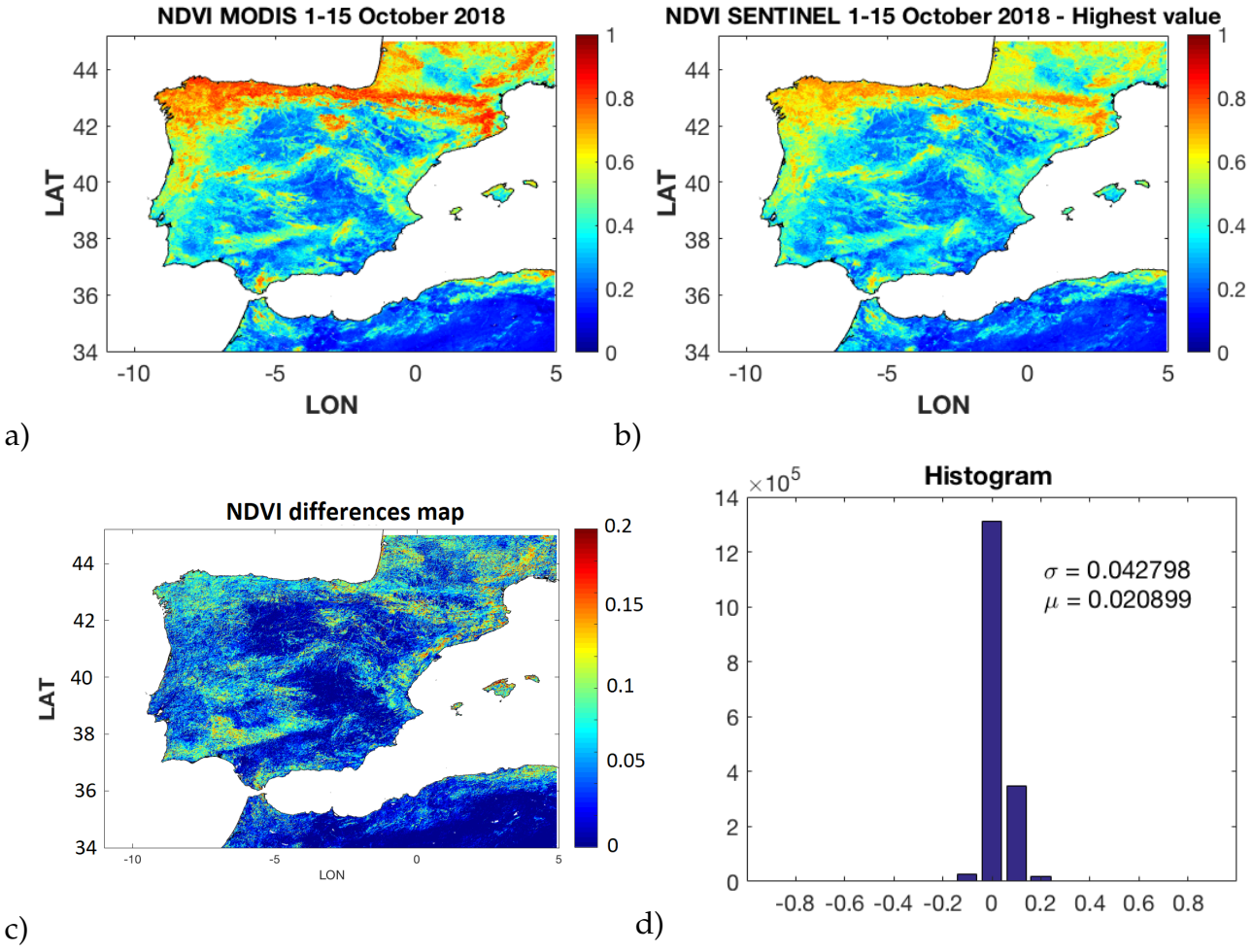

Figure 41: a) and b) are the NDVI from MODIS and Sentinel 3 respectively, c) is the result of the subtraction: Modis NDVI - Sentinel 3 NDVI, and d) is the histogram obtained from c).

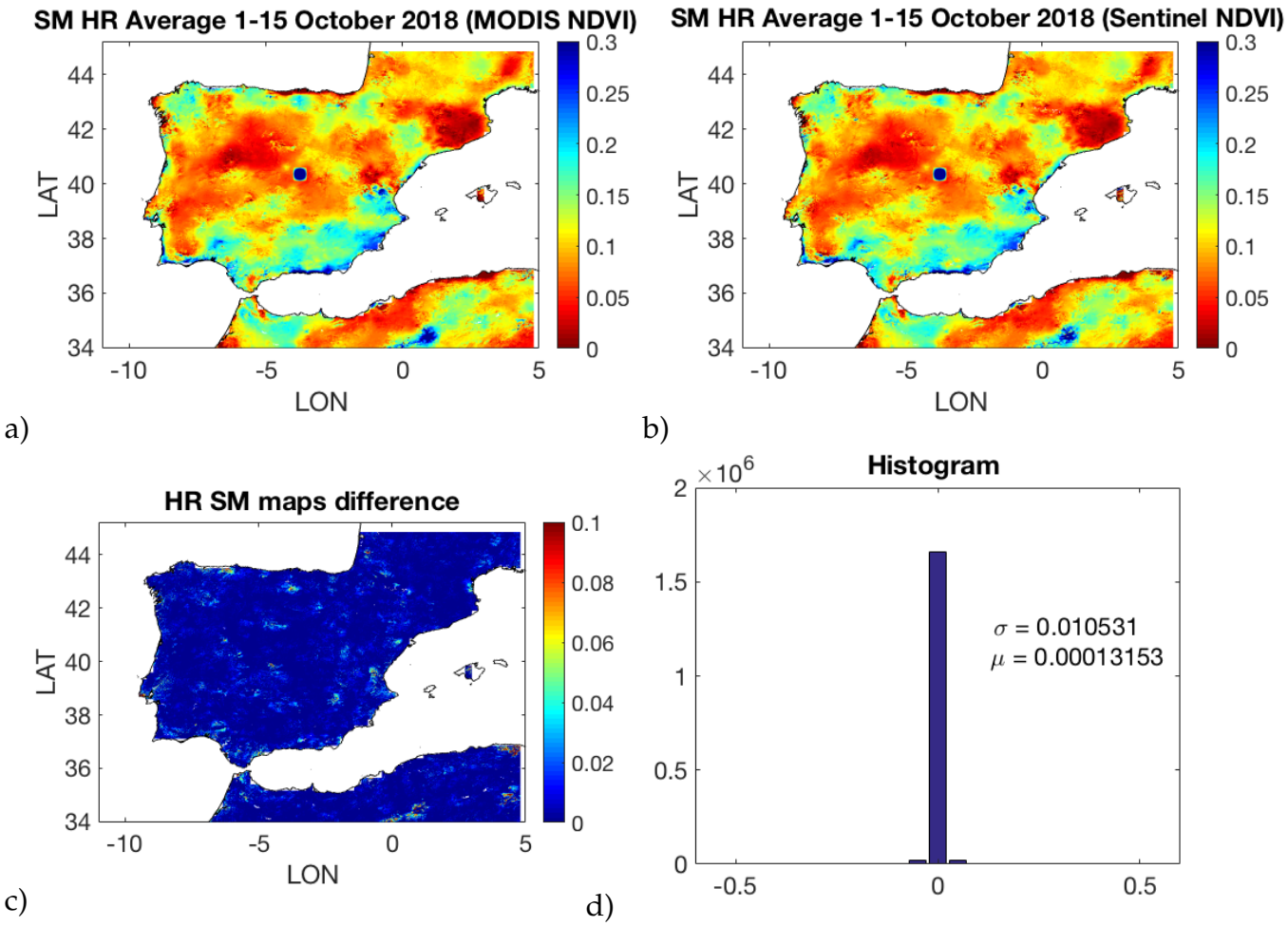

Figure 42: a) and b) are the HR SM maps using NDVI from MODIS and Sentinel 3 respectively, c) is the result of the subtraction: Modis HR SM -Sentinel 3 HR SM, and d) is the histogram obtained from c)

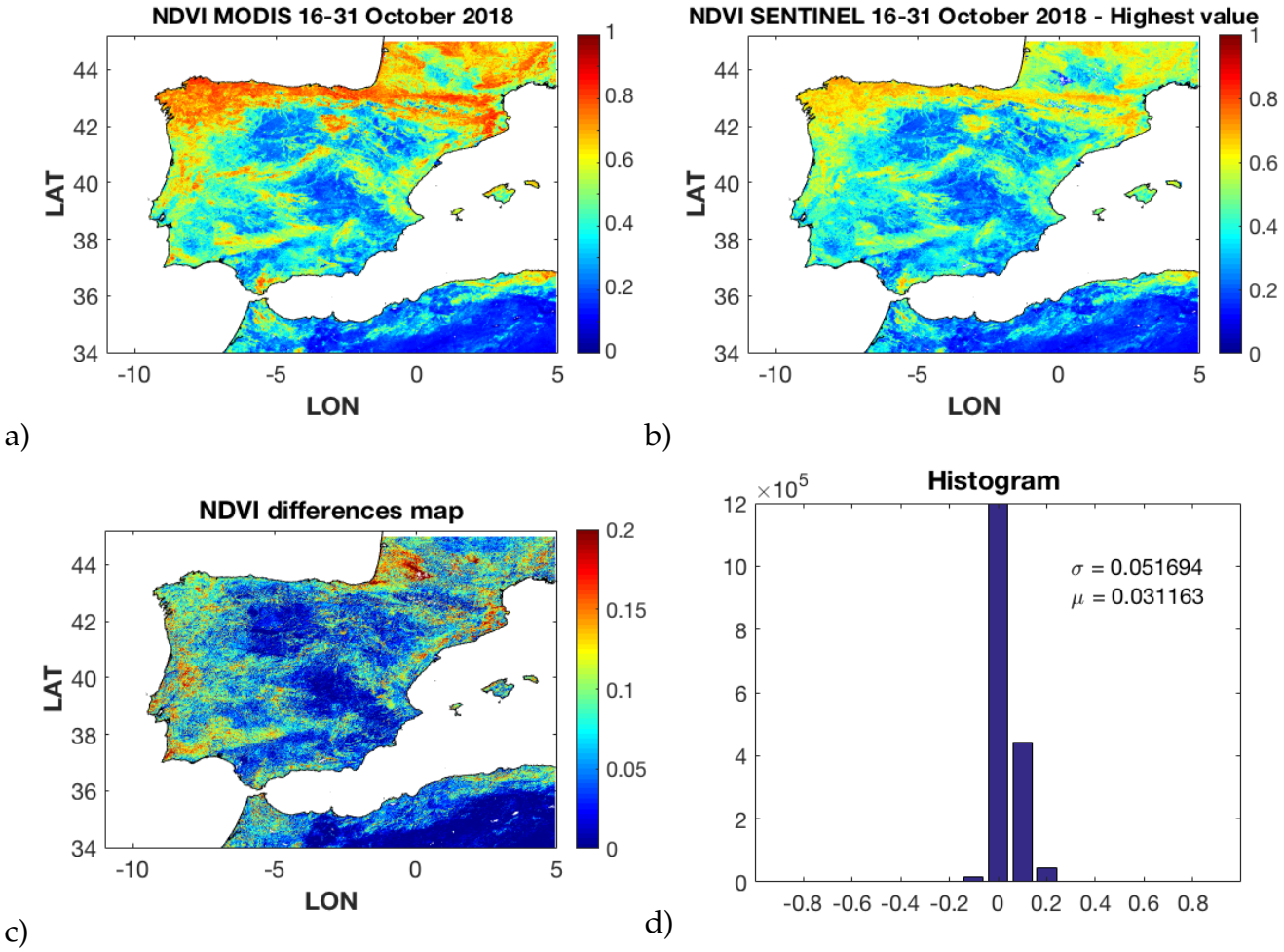

Figure 43: a) and b) are the NDVI from MODIS and Sentinel 3 respectively, c) is the result of the subtraction: Modis NDVI - Sentinel 3 NDVI, and d) is the histogram obtained from c)

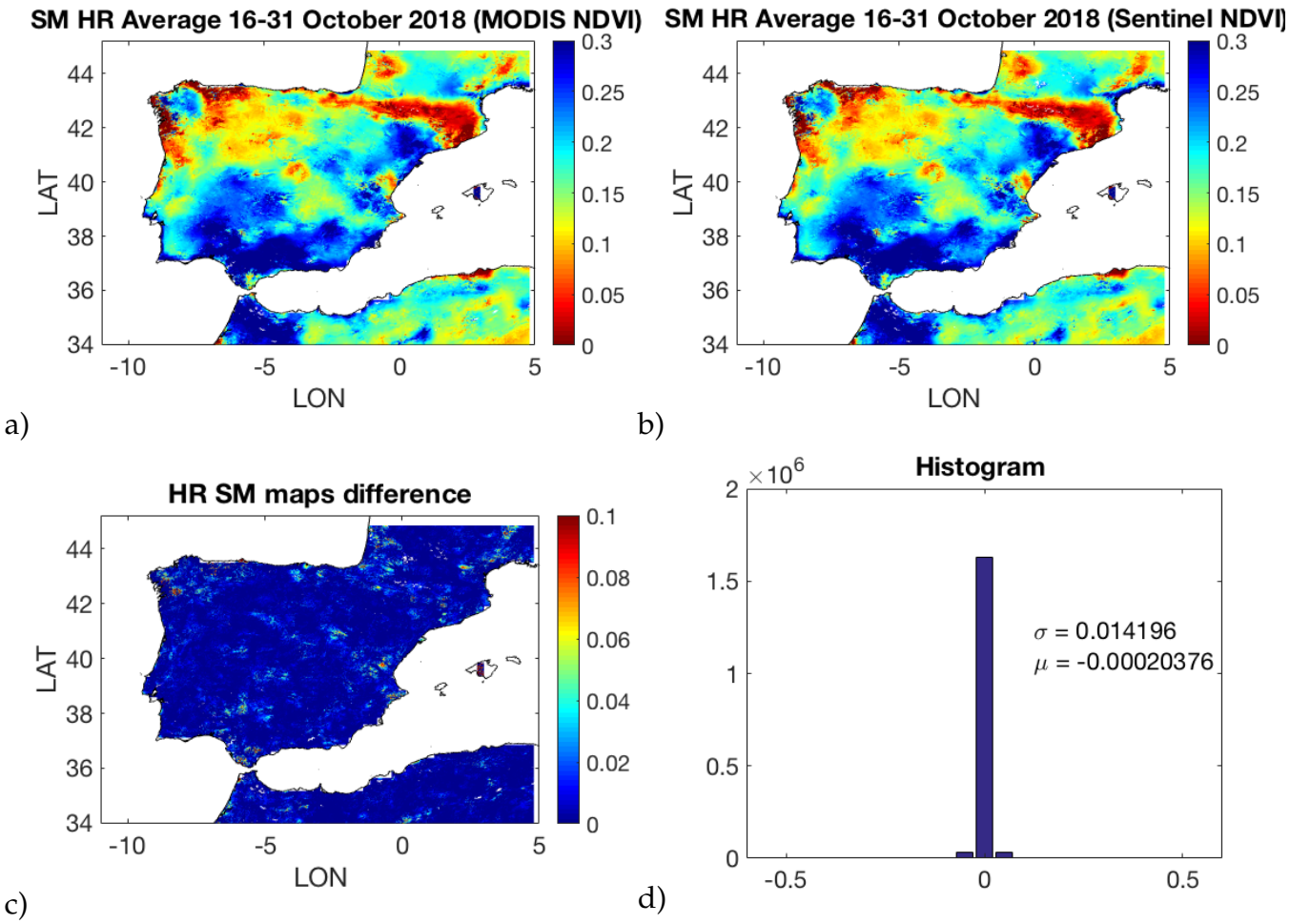

Figure 44: a) and b) are the HR SM maps using NDVI from MODIS and Sentinel 3 respectively, c) is the result of the subtraction: MODIS HR SM -Sentinel 3 HR SM, and d) is the histogram obtained from c).

The NDVI from MODIS and Sentinel 3 differ at first sight as it can be seen in figures 41 and 43. The main cause of the difference is probably the divergence in the 16-day product from MODIS and the built product from daily Sentinel 3 NDVI maps.

The variation in the HR SM map obtained by means of the downscaling algorithm is very small in this case too. The mean error of the HR SM maps are on the order of $\sim 10^{-4}$, similar to the mean error when replacing the LST. Also the standard deviation is in a similar range.

The differences are so small that we can conclude that NDVI from Sentinel 3 data can be used instead of the MODIS one.

6

CONCLUSIONS

6.1 RESULTS SUMMARY

In this chapter we will sum up the conclusions from the whole comparison process between LST and NDVI products provided by MODIS and Sentinel 3. Table 45 summarizes it.

MODIS instrument is on board of Terra and Aqua satellite missions. Both missions are sun synchronous with a near-polar circular orbit. Terra crosses the equator from north to south (descending node) at 10:30 AM local time , while Aqua crosses it from south to north (ascending node) at 1:30 P.M. local time. Together they achieve global coverage in less than one day and individually every $1-2$ days approximately.
Sentinel 3 includes a constellation of two satellites: Sentinel-3A and Sentinel-3B, which have the same orbit but phased +/- 140 degrees. The equator crossing time is from 10:30-11:00 AM local time (descending node). Considering both, the revisit time for SLSTR, the instrument providing the LST and NDVI products, is less than one day. With only one satellite, the revisit time is from 1.5 to 1.8 days.

Both MODIS and Sentinel 3 provide LST product daily.
Regarding NDVI, MODIS provides 16-days products, while Sentinel 3 provides it daily.

The Sentinel 3 Hub provides two different L2 LST products: One is a NRT product, uploaded a few hours after its acquisition and available only for a month in the repository. The second one is the NTC product, containing the whole orbit built by merging and applying specific quality filters to NRT products, and available in the long-term.

Let's focus on the data access and data download processes.
Regarding Sentinel 3, both LST and NDVI are obtained from the LST L2 product by

SLSTR instrument. These products are accessible through the Operational Hub, a web based tool with a user interface that allows to download data from Sentinel 1, 2 and 3 platforms from different geographical areas. The download process is hardly automatizable since even though there is an API, the documentation is limited and this platform still needs to be stabilized.
Regarding MODIS, the data download can be automatized. The platform is more mature and better documented, which facilitates the implementation and enables easier access to help, provided by the community.

It is important to highlight also the data preparation process before using it as ancillay data in the downscaling algorithm.
Before using the LST and NDVI from Sentinel 3 in the downscaling algorithm, it is necessary to convert the files downloaded from the Operational hub to netcdf format. The application that ESA provides to perform this process is called SNAP. Extra processing may be applied to improve the quality of the data by using this application too. SNAP provides the Python module snappy, which allows access to the SNAP Java API from Python. The main handicap using this API is the early stage of the documentation and the small community using it.
If NRT files are used, which is the case in this project, it is necessary to merge the individual tiles of LST and MDVI correspondingly and apply a cloud mask to eliminate the pixels without information due to clouds presence.
Regarding NTC products, it is hard to deal with them in the preparation step since SNAP application requires high computational resources for such big files.

Finally, let's focus in the comparison between LST and NDVI provided by MODIS and Sentinel 3 and the computed HR SM maps using them as ancillary data in the downscaling algorithm.
As demonstrated in section 5, the differences between MODIS and Sentinel LST are very small. For the specific case of October and September 2018, which is the period we studied, the maximum mean error considering 4 days, 15 days and monthly average is 1.3089 K (and 0.11619 K the minimum) and the standard deviation is ~ 2 K approx. The most meaningful variations seem to be caused by the difference in the acquisition time, 12:30-13:30 AM with Aqua and 10:30-11h AM with Sentinel 3.
Replacing the LST from MODIS by the one provided by Sentinel 3 does not lead to meaningful changes in the HR SM obtained. As it can be seen throughout the experiments, the mean error is of the order of 10^{-4} and 10^{-5}. Also, the standard deviation is within the range $0.01 - 0.025$ K.
Regarding NDVI, also the differences in the values provided by the two platforms are small, the mean error and standard deviation are approximately $\sim 0.02 - 0.03$ and ~ 0.05 for October 2018. Also, this variation does not lead to errors or meaningful

differences in the HR SM computation. The mean error is in the order of $\sim 10^{-4}$ for October 2018.

We can conclude that both NDVI and LST from MODIS used as ancillary data in the soil moisture downscaling algorithm, can be replaced by the data from Sentinel 3, being the HR SM maps very similar. So, Sentinel 3 will assure the continuity of MODIS data if it is shut down in the future. Also, if MODIS continues working, they could be used as a together, decreasing the revisit time. The most important handicap of the Sentinel 3 data usage is the maturity of the web platform to download the data and the data preparation platform, SNAP. Both are still on development and need stabilization, there is a lack of documentation and its community is small compared to MODIS community.

	MODIS (Terra and Aqua)	SLSTR (Sentinel 3)
Orbit	Sun-synchronous, near-polar, circular	Sun-synchronous, near polar
Equator crossing time	Terra: 10:30-10:45 AM local time (descending node), 10:30-10:45 P.M. (ascending node) Aqua: 1:30 P.M. local time (ascending node), 1:30 A.M (descending node)	10:00 AM local time (descending node)
Time resolution	1 satellite: 1-2 days 2 satellites: Less than 1 day	1 satellite: - Revisit at equator: < 1.8 days - Revisit for latitude > 30: < 1.5 days 2 satellites: - Revisit at equator: < 0.9 days - Revisit for latitude > 30: < 0.8 days
Spatial resolution	LST and NDVI: 1 km	LST and NDVI: 1 km
Characteristics of the data	LST primary product, daily NDVI primary product, 16-days	LST primary product, daily NDVI ancillary, daily
Data download	Easily automatable	Through web portal: Operations Hub Platform still needs to be stabilized Hardly automatable Small community
Data processing	File format conversion is not necessary. It can be done with Matlab. Size of the tiles is affordable.	Using SNAP tool - Advantages: Easy to use. - Disadvantages: - Lack of documentation - For big files, it demands a lot of resources. Snappy module allows to use SNAP functions into Python code/scripts. - Advantages: It allows to automate the data processing - Disadvantages: - Lack of documentation - Small community
LST and NDVI difference	LST difference range, considering 4 days, 15 days and monthly average (September and October 2018): - mean error range:~ 0.12-1.3 K. - standard deviation: ~2 K NDVI mean difference averaging 16-days (October 2018): - mean error range: ~ 0.02-0.03. - standard deviation: ~ 0.05	
SM HR maps difference	HR SM variation is on the order of ~ $10^{-4} - 10^{-5}$ replacing LST and of ~ 10^{-4} replacing NDVI from MODIS by Sentinel 3 ones in the downscaling algorithm.	

Figure 45: Sentinel 3 vs MODIS

6.2 FUTURE LINES

There are different future lines of investigation:

- Use as ancillary data in the downscaling algorithm the LST provided by era5-land, comparing how it affects the final HR SM maps computed.
- Perform the comparison of HR SM maps obtained when substituting at the same time LST and NDVI from MODIS by the ones from Sentinel 3.
- Extend the comparison of MODIS and Sentinel 3 to other geographical areas with different climate and weather conditions.
- Extend this comparison to all months. This will help to understand whether months with higher or lower temperatures lead to smaller or higher differences. Also, the agriculture conditions change from one month another.

7

BUDGET

In this chapter we describe the necessary resources and the corresponding budget to develop the project.

Regarding human resources, a single graduate engineer has been considered. The approximate salary that an engineer with this attributes would receive is 12 euros/h.

The project has been developed with a Matlab student distribution (R2016b), Python (2.7), SNAP tool and Panoply. For the planning, Teamgantt program has been used.

Regarding hardware, only a PC has been used. According to the resources that SNAP required to process the files, a minimum of 16GB of RAM is necessary for a project with this characteristics.

Find below a table summarizing all resources required for the project and the total cost.

Resource name	Resource type	Notes	Cost (euros)
Engineer	Human	Graduate engineer	9000
Matlab	Software	Version 2016b	Free (academic license)
Python	Software	Version 2.7	Free
SNAP	Software	Version 6.0.0	Free
Office license	Software	Version 2016	140
Teamgantt	Software		Free (trial)
Laptop	Hardware	RAM: 16GB	2500
		Total	11640

Task	Hours (12 euros/h)	Cost (euros)
Analysis and research	300	3600
Implementation/ Adaptation of the algorithm and tests	250	3000
Thesis writing	200	2400
	Total	9000

Figure 46: Resources and cost.

BIBLIOGRAPHY

[1] https://www.aast.edu.

[2] Aqua spacecraft. https://aqua.nasa.gov/content/instruments.

[3] Earth's energy budget. http://sisgeographywiki.mrbgeography.com/3-weather-and-climate/.

[4] European space agency (esa). https://www.esa.int/ESA.

[5] Miras instrument. https://www.redshift-live.com/en/magazine/articles/Astron%C3%A1utica/21191-MIRAS-2.html.

[6] Modis ndvi algorithm. https://lpdaac.usgs.gov/dataset_discovery/modis/modis_products_table/mod13a2_v006.

[7] Planck's law radiation curves. http://how-it-looks.blogspot.com/2010/01/infrared-radiation-black-bodies-and.html.

[8] Sentinel 3 altimetry. https://sentinel.esa.int/web/sentinel/user-guides/sentinel-3-altimetry.

[9] Sentinel 3 olci. https://sentinel.esa.int/web/sentinel/user-guides/sentinel-3-olci.

[10] Sentinel 3 slstr. https://sentinel.esa.int/web/sentinel/user-guides/sentinel-3-slstr.

[11] Sentinel 3 synergy. https://sentinel.esa.int/web/sentinel/user-guides/sentinel-3-synergy.

[12] Sentinel3 pre-operations hub. http://www.esa.int/Our_Activities/Observing_the_Earth/SMOS.

[13] Sentinel3 pre-operations hub. https://scihub.copernicus.eu/s3/#/home.

[14] Slstr otical scanning unit. https://sentinel.esa.int/web/sentinel/technical-guides/sentinel-3-slstr/instrument/description.

[15] Slstr structure. https://sentinel.esa.int/web/sentinel/technical-guides/sentinel-3-slstr/instrument.

[16] A.K, F., and H.J., E. An apprximate model for backscattering and emission from land and sea. *AgRistars* (1981).

[17] Barrett, B.W., D. E. . W. P. Soil moisture retrieval from active spaceborne microwave observations: An evaluation of current techniques. *Remote Sensing, 1*.

[18] Blanchard, B. J., M. M. J. S. T. J., and Rhoades, E. Estimation of soil moisture with api algorithms and microwave emissions. *Water Resour. Bull.17*.

[19] Burke, E.J., B. L., and Shuttleworth, W. Multipatch retrieval for the smos mission. *IEEE Trans. Geosci* (2001).

[20] Delaney, P. H. A. Dielectric properties of soils at uhf and microwave frequencies. *Journal of Geophysical Research* (1974).

[21] Eagleman, J., and Lin, W. Remote sensing of soil moisture by a 21 cm passive radiometer. *Hydrol. Earth Syst. Sci., 80*.

[22] Geiger, F. E., and Williams, D. Dielectric constants of soils at microwave frequencies. *NASA*.

[23] Gerard Portal, Merc Vall-llossera, M. P. A. C. D. C. M. P. L. R. A spatially consistent downscaling approach for smos using an adaptive moving windows.

[24] G.Portal. Application of satellite microwave remote sensed brightness temperature in the regional soil moisture simulation. *ETSETB* (2017).

[25] Hipp, J. E. Soil electromagnetic parameters as a function of frequency, soil density and soil moisture. *Proc. IEEE*.

[26] Hu, Z xu, L. . Y. B. Soil moisture retrieval using convolutional neural networks: Application to poassive microwave remote sensing. *International Archives of the Photogrammetry, Remote Sensing and Spatial Information Sciences. XLII-3*..

[27] Jackson, T. J., . S. T. J. Vegetation effects on the microwave emission of soils. *Remote Sensing of Environment* (1991), 203–212.

[28] Jackson, T. J., S. T. J. . W. J. R. Passive microwave sensing of soil moisture under vegetation canopies. *Water Resources Research 18* (1982), 11371142.

[29] Kirdiashev, K. P., C. A. A. . S. A. M. Microwave radiation of the earth's surface in the presence of vegetation cover. *Radiotekhnika I Elektronika 24* (1979), 256264.

[30] Kornelsen, K. C., C. P. Advances in soil moisture retrieval from synthetic aperture radar and hydrological applications. *Journal of Hydrology, 476* (2013).

[31] Mina Moradizadeh, M. R. Vegetation effects modeling in soil moisture retrieval using msvi. *Photogrammetric Engineering Remote Sensing* (2016).

[32] M.Piles. Multiscale soil moisture retrievals from microwave remote sensing observation. *ETSETB* (2010).

[33] Newton, L. T. R. W. Microwave emissions from soils with rough surfaces. *Agu100*, 87, 9017–9024.

[34] Njokul, E. G., and Entekhabi, D. Passive microwave remote sensing of soil moisture. *Journal of Hydrology* (1994).

[35] Schmugge, T. Microwave remote sensing of soil moisture.

[36] Soares, Joo Renn, C. Soil moisture retrieval from active microwave remote sensing. *European Space Agency, (Special Publication) ESA SP. 407. 195*..

[37] Wang, J.R. Choudhury, B. Remote sensing of soil moisture content over bare field at 1.4 ghz frequency. *ournal of Geophysical Research. 86* (1981).

[38] Wang, J. R., and Schmugge, T. An empirical model for the complex dielectric permittivity of soils as a function of water content. *IEEE Transactions on Geoscience and Remote Sensing*.

[39] Wigneron, J., Y. K. P. W. L-band microwave emission of the biosphere (l-meb) model: description and calibration against experimental data sets over crop fields. *Remote sensing of the environment* (2017), 639–655.

[40] X. K. Shi, J. Wen, L. W. T. T. Z. H. T. X. W. R. L., and Zhang, J. H. A spatially consistent downscaling approach for smos using an adaptive moving window. *Hydrology and Earth System Sciences Discussions* (2009).

[41] Yu, Fan Zhao, Y. A new semi-empirical model for soil moisture content retrieval by asar and tm data in vegetation-covered areas. *SCI CHINA-EARTH SCI. 54*..

[42] Zheng Xingming, Zhao Kai, L. Y. R. J., and Yanling, D. The effect of row structure on soil moisture retrieval accuracy from passive microwave data. *Scientific World Journal* (2014).

[43] ZHENG Xingming, Z. K. A method for surface roughness parameter estimation in passive microwave remote sensing. *Chinese Geographical Science* (2010).

[44] Zhiqiang Gaoa, b, . W. G. b. N.-B. C. Integrating temperature vegetation dryness index (tvdi) and regional water stress index (rwsi) for drought assessment with the aid of landsat tm/etm+ images. *International Journal of Applied Earth Observation and Geoinformation* (2011).